Ocean Engineering 304 (2024) 117771



Contents lists available at ScienceDirect

Ocean Engineering

journal homepage: www.elsevier.com/locate/oceaneng



An efficient procedure for modal seismic response analysis of axisymmetric structures surrounded by water

Ramtin Kouhdasti[1], Najib Bouaanani [*,2]

Department of Civil, Geological and Mining Engineering, Polytechnique Montréal, Montréal, QC H3C 3A7, Canada

ARTICLE INFO

Keywords:
Axisymmetric water–structure systems
Hydrodynamic pressure
Seismic response
Dynamic modal superposition
Modal time-history analysis
Fluid–structure interaction
Simplified methods

ABSTRACT

This paper presents a new procedure for the seismic response assessment of water-surrounded axisymmetric structures through the inclusion of earthquake-induced hydrodynamic effects into input ground motion accelerations. The resulting modified time-history and spectral ground motion accelerations can then be applied directly to the dry axisymmetric structure (*i.e.* without water) through dynamic modal superposition or response spectrum analyses. Therefore, recourse to specialized software accounting for fluid–structure interaction dynamic effects can be avoided. The proposed approach evaluates the individual impact of hydrodynamic effects associated with any specific structural vibration mode on the global structural seismic response. The procedure implements hydrodynamic pressure formulation or simplified added masses as an alternative to classical nodal lumping. A hydrodynamic modification factor to efficiently estimate amplification or de-amplification of acceleration seismic demands due to earthquake-induced hydrodynamic effects is proposed. The application of the proposed methods is illustrated numerically through examples of three water-surrounded axisymmetric structures subjected to two earthquakes. The results of key response indicators, including relative displacements, base shear, and stresses are shown to be in excellent agreement with the coupled finite element solutions. The coupled effects of hydrodynamic-pressure and structural flexibility on the seismic behaviour of the studied systems are discussed.

1. Introduction

The seismic response of axisymmetric water-surrounded structures can be affected by earthquake-induced hydrodynamic pressure and fluid–structure interaction. This topic has been extensively covered by many researchers (*e.g.* Liaw and Chopra, 1974; Taylor and Duncan, 1980; Williams, 1986; Tanaka and Hudspeth, 1988; Wei et al., 2015; Yang et al., 2017; Alembagheri, 2017; Wang et al., 2018b; Zhang et al., 2019; Tian et al., 2020; Sun et al., 2020; Wang et al., 2021; Li et al., 2022; Han et al., 2023). Analytical solutions for hydrodynamic pressures on an elastic cylindrical tower based on radiation wave theory have been developed including water compressibility (Liaw and Chopra, 1974; Tanaka and Hudspeth, 1988; Greenhow and Yanbao, 1987; Wang et al., 2022; Wu et al., 2023a; Huang et al., 2023). Simplified added mass formulations simulating hydrodynamic effects have also been proposed (Westergaard, 1933; Liaw and Chopra, 1974; Greenhow and Yanbao, 1987; Li and Yang, 2013; Jiang et al., 2017; Zhang et al., 2019; Wang et al., 2018a). Morison's equation has gained widespread acceptance to evaluate hydrodynamic effects on slender cylinders due to its simplicity (Yang and Li, 2013; Liu and Sun, 2014; Zheng et al., 2015; Li et al., 2017; Wu et al., 2023b). Originally proposed by Morison et al. (1950) for calculating wave loads, this semi-empirical formula was later modified by Penzien and Kaul (1972) to account for hydrodynamic forces on cylindrical structures during earthquakes. Numerical techniques such as finite element, boundary element, and scaled boundary element methods are other common alternatives widely used to investigate earthquake-induced hydrodynamic effects on axisymmetric water-surrounded structures (*e.g.* Everstine, 1981; Olson and Bathe, 1985; Chen, 2000; Czygan and Von Estorff, 2002; Sigrist and Garreau, 2007; Millán et al., 2009; Lu and Jeng, 2010; Tao et al., 2007; Meng and Zou, 2012; Liu and Lin, 2013; Xu et al., 2023; Padrón et al., 2022; Bigdeli et al., 2023). These techniques generally allow for the coupling of structural and hydrodynamic responses through fluid–structure interface elements. However, implementing such coupled solutions often requires specialized software, extensive time necessary to build and execute the models, and a considerable level of expertise to ensure reliable and accurate results

* Corresponding author.
E-mail address: najib.bouaanani@polymtl.ca (N. Bouaanani).
[1] Ph.D. Student.
[2] Professor.

https://doi.org/10.1016/j.oceaneng.2024.117771
Received 26 December 2023; Received in revised form 16 March 2024; Accepted 2 April 2024
Available online 22 April 2024
0029-8018/© 2024 The Authors. Published by Elsevier Ltd. This is an open access article under the CC BY-NC-ND license (http://creativecommons.org/licenses/by-nc-nd/4.0/).

(Liaw and Chopra, 1974; Goyal and Chopra, 1989; Bouaanani and Lu, 2009; Wei et al., 2015).

Despite the multitude of available methods for the seismic analysis of water-surrounded axisymmetric structures, engineering practice still needs new alternative techniques with a fair balance between complexity, efficiency, and simplicity of application and interpretation of the obtained results. The semi-analytical approach proposed in this paper breaks down earthquake-induced hydrodynamic effects on the seismic response of the studied water–structure system along multiple vibration modes of the dry structure (*i.e.* without water). This process enables a better understanding of the impact of each mode and associated hydrodynamic effects of the global seismic response. For this purpose, a methodology is developed to include earthquake-induced hydrodynamic effects into input ground motion accelerations. The resulting modified time–history and spectral ground motion accelerations can then be applied directly to the dry axisymmetric structure through dynamic modal superposition or response spectrum analyses. Therefore, recourse to specialized software accounting for fluid–structure interaction dynamic effects can be avoided. The procedure implements hydrodynamic pressure formulation or simplified added masses as an alternative to classical nodal lumping.

The article is structured as follows. First, the theoretical background of the proposed method is presented, as well as detailed procedures illustrating the application of the proposed dynamic modal superposition and response spectrum analyses. Numerical case studies of three axisymmetric structures with different heights are presented and the results of key response indicators, including relative displacements, base shear, and stresses are discussed and compared to classical coupled finite element solutions accounting for dynamic fluid–structure interaction.

2. Theoretical background and proposed methods

2.1. Basic assumption and governing equations

An axisymmetric structure, as the one depicted in Fig. 2(a), is considered to illustrate the procedure proposed. The structure has a total height H_s and is surrounded by an infinite water domain with a constant depth H_w. The submerged section of the structure has a uniform outer radius R_s. Two coordinate systems are employed to define the geometry: (i) a Cartesian system (x, y, z), originating at the centre of the bottom cross-section of the structure, with the z-axis aligning with the axis of symmetry; and (ii) a cylindrical system (r, θ, z), where r represents the radial distance and θ the azimuth between the reference x-axis and the line from the origin to the projection of the point of interest on the (x, y) plane. The structure's dynamic response is analysed under the effect of a horizontal ground motion acceleration $\ddot{x}_g(t)$ applied along the x-direction. The axisymmetric structure can be composed of one or more materials and its cross-section can be solid or hollow, with uniform or varying internal radius. The following main assumptions are made: (i) all constitutive materials exhibit linear elastic behaviour during seismic excitation, (ii) water is assumed to be inviscid, but can be compressible or incompressible, with its motion irrotational and of small amplitudes, (iii) convective effects and surface gravity waves in water are neglected, and (iv) the foundation is massless and rigid.

It can be shown that dynamic behaviour of the axisymmetric water–structure tower subjected to a unit horizontal harmonic ground acceleration $\ddot{x}_g(t) = e^{i\omega t}$, with ω denoting the forcing frequency, can be determined through the solution of a system of equations (Liaw and Chopra, 1974; Wei et al., 2015)

$$\hat{\mathbf{S}}\,\hat{\mathbf{Z}} = \hat{\mathbf{Q}} \tag{1}$$

in which $\hat{\mathbf{Z}}$ denotes the vector of generalized coordinates $\hat{Z}_j$, and the elements of the matrix $\hat{\mathbf{S}}$ and vector $\hat{\mathbf{Q}}$ are given for $m = 1 \dots N_s$ and $j = 1 \cdots N_s$ as

$$\hat{S}_{j,m}(\omega) = \left(-\omega^2 + 2\,i\,\xi_j\,\omega\,\omega_j + \omega_j^2\right) M_j\,\delta_{j,m} - \omega^2\,\vartheta_{j,m}(\omega) \tag{2}$$

$$\hat{Q}_m(\omega) = -L_m^{(x)} - \vartheta_{0,m}(\omega) \tag{3}$$

where $\delta_{j,m}$ denote the Kronecker symbol, ω_j the natural vibration frequency corresponding to structural mode $\boldsymbol{\psi}_j$ of the dry structure, *i.e.* without water, ξ_j the fraction of critical damping, $M_j = \boldsymbol{\psi}_j^T \mathbf{M}\,\boldsymbol{\psi}_j$ the generalized modal mass, $L_m^{(x)} = \boldsymbol{\psi}_m^T \mathbf{M}\,\mathbf{1}^{(x)}$ the horizontal modal participation factor, with $\mathbf{1}^{(x)}$ a column-vector containing zeros except along horizontal degrees of freedom corresponding to earthquake direction, and where the parameters $\vartheta_{0,m}(\omega)$ and $\vartheta_{j,m}(\omega)$ are given by

$$\vartheta_{0,m}(\omega) = R_s \int_0^{H_w} \int_0^{2\pi} p_0(R_s, \theta, z, \omega)\,\cos(\theta)\,\psi_m^{(x)}(R_s, 0, z)\,d\theta\,dz \tag{4}$$

$$\vartheta_{j,m}(\omega) = R_s \int_0^{H_w} \int_0^{2\pi} p_j(R_s, \theta, z, \omega)\,\cos(\theta)\,\psi_j^{(x)}(R_s, 0, z) \times \psi_m^{(x)}(R_s, 0, z)\,d\theta\,dz \quad \text{for} \quad j, m = 1 \dots N_s \tag{5}$$

with p_0 denoting the hydrodynamic pressure FRF at *rigid* structure–water interface due to horizontal ground motion $\ddot{x}_g$ and p_j the hydrodynamic pressure FRF at *flexible* structure–water interface due to horizontal acceleration $\psi_j^{(x)}(R_s, 0, z)$, $j = 1 \cdots N_s$. The FRFs p_0 and p_j can be evaluated using the expressions given in Appendix.

The previous equations are based on the modelling of earthquake-induced water effects through hydrodynamic pressures interacting with the vibrating structure. When hydrodynamic effects are modelled using the simplified formulation of added masses (Liaw and Chopra, 1974), Eqs. (4) and (5) can be substituted as follows

$$\vartheta_{0,m} = R_s \int_0^{H_w} \int_0^{2\pi} p_0(R_s, \theta, z)\,\cos(\theta)\,\psi_m^{(x)}(R_s, 0, z)\,d\theta\,dz \tag{6}$$

$$\vartheta_{j,m} = R_s \int_0^{H_w} \int_0^{2\pi} p_0(R_s, \theta, z)\,\cos(\theta)\,\psi_j^{(x)}(R_s, 0, z)\,\psi_m^{(x)}(R_s, 0, z)\,d\theta\,dz \tag{7}$$

where $p_0(R_s, \theta, z)$ can be interpreted as the water added mass per unit height of the structure (Liaw and Chopra, 1974). Alternatively to this formulation based on the radiation wave theory, water added masses can also be expressed using Morison's equation (Morison et al., 1950; Penzien and Kaul, 1972). Assuming that the terms associated with drag force and hydrodynamic damping can be neglected (Guo et al., 2021), Eqs. (4) and (5) can be shown to simplify to

$$\vartheta_{0,m} = \pi\,\rho_w\,R_s^2 \int_0^{H_w} \psi_m^{(x)}(R_s, 0, z)\,dz \tag{8}$$

$$\vartheta_{j,m} = \pi\,\rho_w\,R_s^2 \int_0^{H_w} \psi_j^{(x)}(R_s, 0, z)\,\psi_m^{(x)}(R_s, 0, z)\,dz \quad \text{for} \quad j, m = 1 \cdots N_s \tag{9}$$

The total horizontal relative displacement $\hat{u}$ and acceleration $\ddot{\hat{u}}$ at a point (x, y, z) of the water-surrounded axisymmetric structure can be computed as the summation of modal contributions

$$\hat{u}(x, y, z, t) = \sum_{j=1}^{N_s} \hat{u}_j(x, y, z, t) = \sum_{j=1}^{N_s} \hat{Z}_j(t)\,\psi_j^{(x)}(x, y, z) \tag{10}$$

$$\ddot{\hat{u}}(x, y, z, t) = \sum_{j=1}^{N_s} \ddot{\hat{u}}_j(x, y, z, t) = \sum_{j=1}^{N_s} \ddot{\hat{Z}}_j(t)\,\psi_j^{(x)}(x, y, z) \tag{11}$$

where $\hat{u}_j$ and $\ddot{\hat{u}}_j$ denote the modal relative horizontal displacement and acceleration at a point (x, y, z) of water-surrounded axisymmetric structure subjected to original ground acceleration $\ddot{x}_g$.

The dynamic response of the structure without water can be obtained as the superposition of N_s responses of equivalent single degree-of-freedom (ESDOF) systems with generalized coordinates along the x-direction Z_j satisfying (Fenves and Chopra, 1984; Bouaanani and Perrault, 2010; Liaw and Chopra, 1974; Wei et al., 2015)

$$Z_j(\omega) = -\frac{L_j^{(x)}}{M_j} \times \frac{1}{\left(-\omega^2 + 2\,i\,\xi_j\,\omega\,\omega_j + \omega_j^2\right)} \tag{12}$$

The total horizontal relative displacement u and acceleration $\ddot{u}$ at a point (x, y, z) of the structure without surrounding water can be computed as the summation of modal contributions

$$u(x,y,z,t) = \sum_{j=1}^{N_s} u_j(x,y,z,t) = \sum_{j=1}^{N_s} Z_j(t)\,\psi_j^{(x)}(x,y,z) \tag{13}$$

$$\ddot{u}(x,y,z,t) = \sum_{j=1}^{N_s} \ddot{u}_j(x,y,z,t) = \sum_{j=1}^{N_s} \ddot{Z}_j(t)\,\psi_j^{(x)}(x,y,z) \tag{14}$$

with u_j and $\ddot{u}_j$ denote the modal relative horizontal displacement and acceleration at a point (x, y, z) of the dry structure (*i.e.* without water) considering a unit harmonic horizontal ground motion $\ddot{x}_g(t) = e^{i\omega t}$.

The previous equations were developed under the assumption of a unit horizontal harmonic ground acceleration $\ddot{x}_g(t)$. In the general case, the Fourier transform of a given ground motion acceleration $\ddot{x}_g(t)$ can be determined as

$$\ddot{x}_g(\omega) = \int_0^{t_a} \ddot{x}_g(t)\, e^{-i\omega t}\, dt \tag{15}$$

in which t_a is the time duration of the applied accelerogram. The total horizontal relative displacements $\hat{u}$ and u of the system with and without surrounding water, respectively, subjected to ground motion acceleration $\ddot{x}_g(t)$ can be expressed in the frequency domain as

$$\hat{u}(x,y,z,\omega) = \ddot{x}_g(\omega) \sum_{j=1}^{N_s} \hat{u}_j(x,y,z,\omega) = \ddot{x}_g(\omega) \sum_{j=1}^{N_s} \hat{Z}_j(\omega)\,\psi_j^{(x)}(x,y,z) \tag{16}$$

$$u(x,y,z,\omega) = \ddot{x}_g(\omega) \sum_{j=1}^{N_s} u_j(x,y,z,\omega) = \ddot{x}_g(\omega) \sum_{j=1}^{N_s} Z_j(\omega)\,\psi_j^{(x)}(x,y,z) \tag{17}$$

2.2. Proposed formulations

A mode- and frequency-dependent ground motion acceleration $a_g^{(j)}$ is defined by modifying the original input ground motion acceleration $\ddot{x}_g(\omega)$ as follows

$$a_g^{(j)}(\omega) = \ddot{x}_g(\omega)\,\frac{\hat{Z}_j(\omega)}{Z_j(\omega)} \quad \text{for} \quad j = 1 \cdots N_s \tag{18}$$

The modal horizontal relative displacements $\widetilde{u}_j$ at a point (x, y, z) of the dry structure subjected to modified ground motion acceleration $a_g^{(j)}$ can be expressed as

$$\widetilde{u}_j(x,y,z,\omega) = a_g^{(j)}(\omega)\, Z_j(\omega)\,\psi_j^{(x)}(x,y,z) = \ddot{x}_g(\omega)\,\hat{Z}_j(\omega)\,\psi_j^{(x)}(x,y,z) \tag{19}$$

Comparing with Eq. (10), it is seen that these modal relative displacement and acceleration are the same as those of the water–structure system subjected to the original ground acceleration $\ddot{x}_g$, *i.e.* $\widetilde{u}_j = \hat{u}_j$ and $\ddot{\widetilde{u}}_j = \ddot{\hat{u}}_j$. Applying Fourier inverse transform to $a_g^{(j)}(\omega)$ yields the following modified time–history ground acceleration for each structural mode $j = 1 \cdots N_s$

$$a_g^{(j)}(t) = \frac{1}{2\pi} \int_{-\infty}^{\infty} a_g^{(j)}(\omega)\, e^{i\omega t}\, d\omega \tag{20}$$

This accelerogram can be directly applied to the dry structure to obtain the contribution of any given mode j to the time–history response of the wet structure (*i.e.* with water) through the solution of the equation

$$\ddot{\widetilde{Z}}_j(t) + 2\,\xi_j\,\omega_j\,\dot{\widetilde{Z}}_j(t) + \omega_j^2\,\widetilde{Z}_j(t) = -\frac{L_j^{(x)}}{M_j}\,a_g^{(j)}(t) \quad \text{for} \quad j = 1 \cdots N_s \tag{21}$$

for the generalized coordinate $\widetilde{Z}_j(t)$. In other terms, the solution of Eq. (21) is the same as the solution of the system with water subjected to original ground acceleration, i.e $\widetilde{Z}_j(t) = \hat{Z}_j(t)$. This method is shown in Fig. 1(a), where the seismic response of an axisymmetric water-surrounded structure is obtained through the superposition of the time–history modal dynamic responses (*i.e.* Time–history modal superposition analysis abbreviated as THMSA hereafter) of the tower without water (dry system) subjected to modified ground accelerations $a_g^{(j)}(t)$, $j = 1 \ldots N_s$ (Note: $N_s = 4$ modes are considered in Fig. 1 for illustration purposes). In a finite element analysis (FEA), such procedure consists of conducting a time–history modal dynamic analysis of the dry structure (i.e without water) including only the contribution of vibration mode j of concern. The solutions $\widetilde{Z}_j(t)$ of Eq. (21) can be obtained for each mode $j = 1 \cdots N_s$ as the time–history relative displacements of single degree-of-freedom (SDOF) systems with mass M_j, stiffness

$$K_j = \frac{4\pi^2}{T_j^2}\,M_j \tag{22}$$

and viscous damping

$$C_j = \frac{4\pi}{T_j}\,\xi_j\,M_j \tag{23}$$

while subjected to ground motion acceleration $L_j^{(x)}\,a_g^{(j)}(t)$. This procedure is illustrated in Fig. 1(b).

The maximum (*i.e.* peak) absolute seismic horizontal relative displacement of the water-surrounded axisymmetric structure corresponding to a given vibration mode $j = 1 \cdots N_s$ can then be evaluated as

$$\begin{aligned} \left|\hat{u}_j(x,y,z,t)\right|^{(\max)} &= \left|\widetilde{u}_j(x,y,z,t)\right|^{(\max)} \\ &= \frac{L_j^{(x)}}{M_j}\,S_D^{[a_g^{(j)}]}(T_j,\xi_j)\,\psi_j^{(x)}(x,y,z) \\ &= \frac{L_j^{(x)}}{M_j}\,\frac{T_j^2}{4\pi^2}\,S_A^{[a_g^{(j)}]}(T_j,\xi_j)\,\psi_j^{(x)}(x,y,z) \end{aligned} \tag{24}$$

in which $S_D^{[a_g^{(j)}]}(T_j,\xi_j)$ and $S_A^{[a_g^{(j)}]}(T_j,\xi_j)$ denote, respectively, the spectral displacement and pseudo-acceleration of ground motion $a_g^{(j)}(t)$ at the period T_j of the structure without water, considering a modal viscous damping ξ_j. This approach is illustrated in Fig. 1(c).

The maximum absolute total horizontal relative displacement at a point of coordinates (x, y, z) of the structure can then be obtained using a combination rule such as the Square Root of the Sum of the Squares (SRSS)

$$\left|\hat{u}(x,y,t)\right|^{(\max)} = \sqrt{\sum_{j=1}^{N_s}\left[\left|\hat{u}_j(x,y,z,t)\right|^{(\max)}\right]^2} \tag{25}$$

or the complete quadratic combination (CQC)

$$\left|\hat{u}(x,y,t)\right|^{(\max)} = \sqrt{\sum_{j=1}^{N_s}\sum_{m=1}^{N_s} A_{j,m}\left|\hat{u}_j(x,y,z,t)\right|^{(\max)}\left|\hat{u}_m(x,y,z,t)\right|^{(\max)}} \tag{26}$$

where $A_{j,m}$ is the correlation coefficient

$$A_{j,m} = \frac{1}{1+\epsilon_{j,m}^2} \tag{27}$$

in which

$$\epsilon_{j,m} = \frac{\omega_j\sqrt{(1-\xi_j^2)} - \omega_m\sqrt{(1-\xi_m^2)}}{\xi_j'\,\omega_j + \xi_m'\,\omega_m}, \qquad \xi_j' = \xi_j + \frac{2}{\omega_j\,s} \tag{28}$$

with s representing the duration of the strong phase of the earthquake excitation. For systems with the same damping ratio in all modes subjected to earthquake excitation with duration s long enough (*i.e.* $\xi_j' = \xi_j$), Eq. (27) can be simplified to

$$A_{j,m} = \frac{\xi^2(1+\omega_j/\omega_m)^2}{(1-\omega_j/\omega_m)^2 + 4\,\xi^2\,\omega_j/\omega_m} \tag{29}$$

When applicable, the above combination rules or similar can be used to obtain other response quantities of interest.

It is worth mentioning that the maximum absolute seismic horizontal relative displacement of the structure without surrounding water

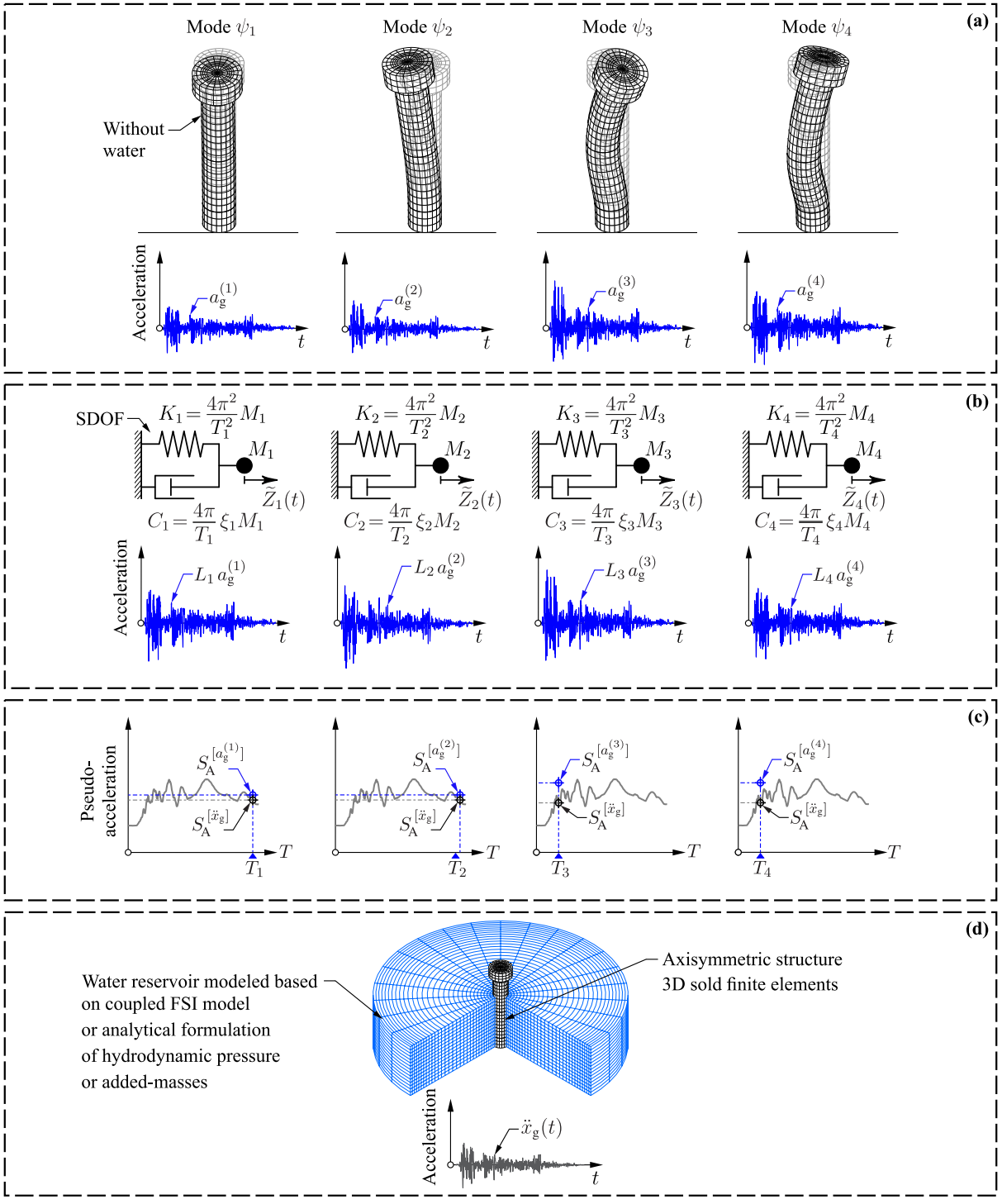


Fig. 1. Proposed procedures.

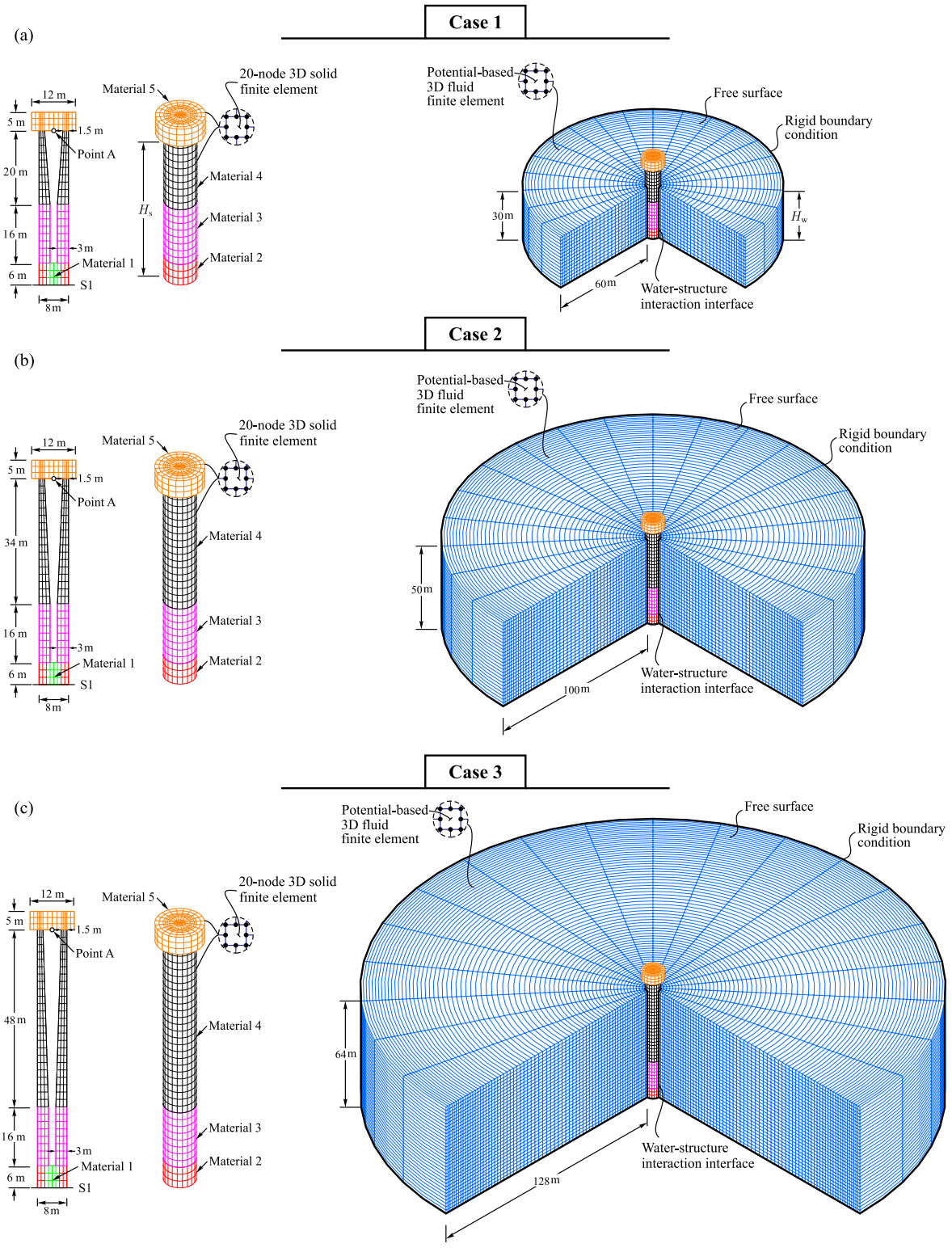


Fig. 2. Dimensions, materials and finite element meshes of the studied water-surrounded axisymmetric structures: (a) Case no. 1 - 42-m height tower; (b) Case no. 2 - 56-m height tower; (c) Case no. 3 - 70-m height tower.

subjected to original ground motion acceleration can be expressed for each structural mode j as

$$\left|u_j(x,y,z,t)\right|^{(\max)} = \frac{L_j^{(x)}}{M_j}\frac{T_j^2}{4\pi^2} S_{\mathrm{A}}^{[\ddot{x}_g]}(T_j,\xi_j)\,\psi_j^{(x)}(x,y,z) \tag{30}$$

From Eqs. (24) and (30), it can be seen that, the ratio of maximum absolute seismic horizontal relative displacements with and without water at a given mode j is equal to the ratio of the pseudo-acceleration of the modified record corresponding to mode j to that of the original ground motion acceleration, *i.e.*

$$\frac{\left|\widetilde{u}_j(x,y,z,t)\right|^{(\max)}}{\left|u_j(x,y,z,t)\right|^{(\max)}} = \frac{S_{\mathrm{A}}^{[a_g^{(j)}]}(T_j,\xi_j)}{S_{\mathrm{A}}^{[\ddot{x}_g]}(T_j,\xi_j)} \quad \text{for} \quad j=1\ldots N_s \quad \text{and} \quad z>0 \tag{31}$$

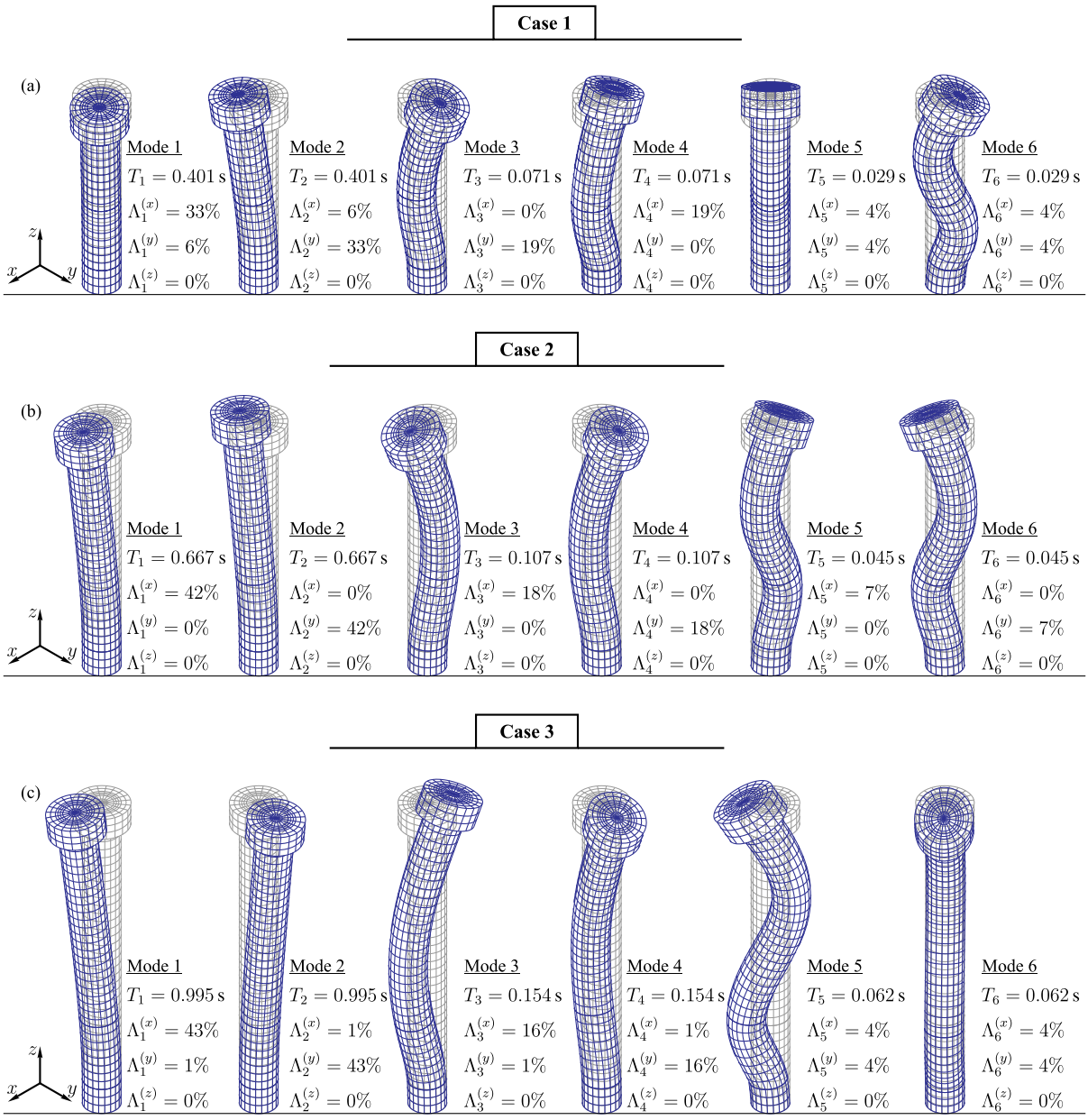


Fig. 3. Finite element mode shapes and corresponding vibration periods of the towers, as well as the modal mass participation factors: (a) Case no. 1; (b) Case no. 2; (c) Case no. 3.

In what follows, the ratio defined by Eq. (31) will be referred to as the *hydrodynamic modification factor* for a given vibration mode, and abbreviated as HMF. The proposed formulations and resulting HMF only require the evaluation of the period and damping corresponding to a specific vibration mode of the structure without surrounding water, rather than those of the water–structure system which are generally different.

3. Numerical examples, results and discussion

3.1. Case studies

Three composite axisymmetric cylindrical towers with different heights are considered in this section to illustrate the application of the proposed methods. The three towers, illustrated in Fig. 2, are referred to as Cases no. 1 to 3, have the same external radius $R_s = 4$ m, and heights H_s of 42 m, 56 m, and 70 m, respectively. The top of the towers are made of a solid cylindrical part with a height of 5 m and a diameter of 12 m. Table 1 contains the mechanical properties of the towers. The towers in Cases no. 1 to 3 are surrounded by an infinite water domain with heights H_w of 30 m, 50 m and 64 m, respectively. A water mass density $\rho_w = 1000$ kg/m^3, a pressure wave velocity $C_w = 1440$ m/s are considered. Fig. 3 presents the six lateral mode shapes and corresponding vibration periods (T_1 to T_6) for the three dry structures, as well as the modal mass participation factors along x, y and z, *i.e.* $\Lambda_j^{(x)}$, $\Lambda_j^{(y)}$ and $\Lambda_j^{(z)}$, respectively, indicating the relative importance of each mode in the global seismic response of the structures. A constant 5% modal viscous damping ratio is considered, *i.e.* $\xi_j = 0.05$ for $j = 1$ to 6. To verify the results, coupled 3D finite element analyses of the tower-water systems are also conducted. The towers and surrounding water are modelled in ADINA (2022) using 3D 20-node solid and potential-based finite elements, respectively, as shown in Fig. 2. A fixed rigid wall boundary condition is applied at a far end located at a radius of $2H_w$ around the structures. Fluid–structure interaction is accounted for through special interface elements included in ADINA (ADINA,

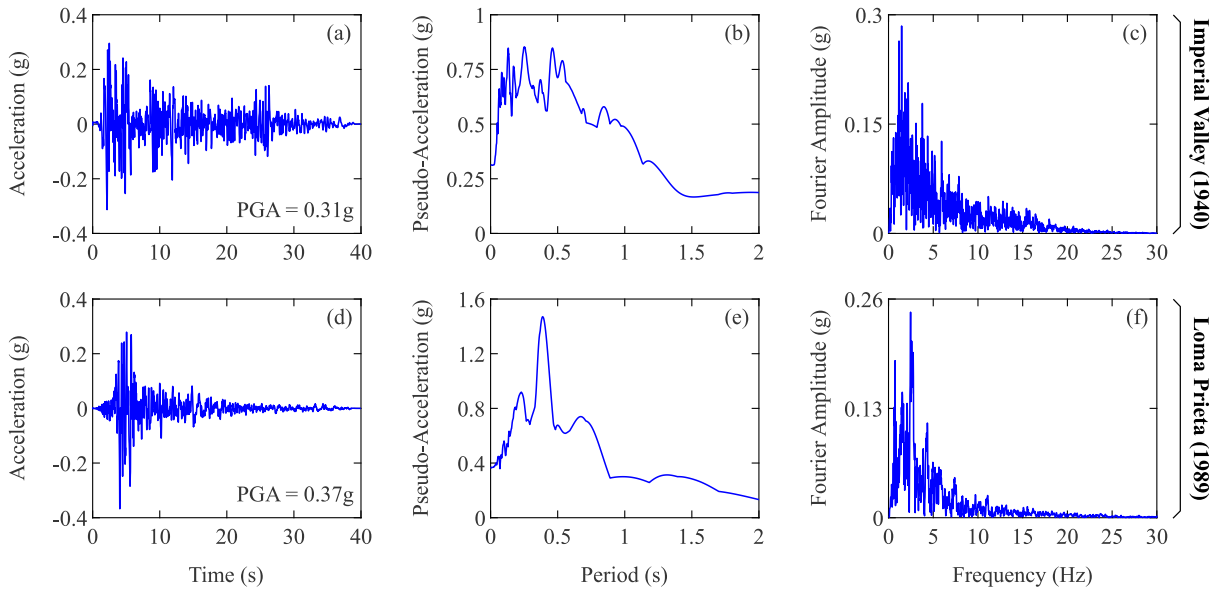


Fig. 4. Time-history accelerations, pseudo-acceleration response spectra and Fourier amplitudes of the ground motions selected for this study: (a) to (c) Imperial Valley (1940) earthquake; (d) to (f) Loma Prieta (1989) earthquake.

Table 1
Constitutive materials of the axisymmetric structures (Fig. 2).

Materials	Mass density (kg/m^3)	Elastic modulus (GPa)	Poison's ratio
Material 1	7850	210	0.3
Material 2	2400	35	0.2
Material 3	2500	25	0.2
Material 4	1900	50	0.2
Material 5	2400	30	0.2

2022; Bouaanani and Lu, 2009). In the following discussion, the results of the coupled finite element models are referred to as the reference solution, also illustrated in Fig. 1(d).

Fig. 5, shows the frequency response functions (FRFs) for horizontal acceleration $\hat{\ddot{u}}$ and $\ddot{u}$ at point A of studied structures. Two water levels H_w and $0.5H_w$ are considered as well as the dry case for comparison purposes. The blue curves represent the FRFs of the towers surrounded by water, while the grey curves depict those of the towers without water. Comparing these results shows that the FRFs generally shift toward lower frequencies from the dry case to the case with a water level of $0.5H_w$, and then H_w. This expected behaviour confirms that the system becomes generally more flexible with higher water levels. The influence of water level must however be considered in light of the frequency content of the seismic excitation. For example, according to the FRFs in Fig. 5, a ground motion with a predominant exciting frequency of 3 Hz results in the same horizontal acceleration response for Case no. 1 irrespective of the water level. The same applies to Cases nos. 2 and 3. However, at a predominant excitation frequency of 6 Hz, the effect of water level is obvious from Fig. 5(e) for Case no. 3, while this effect vanishes for Case no. 1 as shown in Fig. 5(a).

3.2. Original and modified ground motions used

The seismic response of each tower is studied under the effects of two ground motion accelerations differing by their frequency content and time signature: (i) a horizontal component of Imperial Valley earthquake (1940) at station El Centro, (ii) a horizontal component of Loma Prieta earthquake (1989) at station Gilroy Array no. 2. The acceleration time-histories, acceleration pseudo-spectra and Fourier amplitudes of these ground motions are illustrated in Fig. 4. The modified accelerograms corresponding to both records are compared to the original ground motions in Figs. 6 and 7 for the three cases assuming compressible water. Fig. 8 illustrates the impact of different water assumptions on the generated modified accelerograms of Imperial Valley (1940) earthquake for the three cases. It is observed that the different water assumptions yield closely similar results for the shortest tower (Case no. 1). As structural flexibility increases (Cases nos. 1 and 2), the simplified added mass using Morison equations exhibit higher discrepancies compared to the ones with compressible water assumption. The added masses based on radiation wave theory yield modified accelerations closer to those using compressible water assumption than the Morison's added mass formulation. In this figure, the effects of Morison's added mass on the modified ground acceleration for each mode can be observed. Notably, a larger peak ground acceleration (PGA) for higher modes is achieved through Morison's added masses formulation.

The pseudo-acceleration response spectra $S_A^{[a_g^{(j)}]}(T_j, 5\%)$, $j = 1 \dots 6$, of the modified ground accelerations are computed for the six vibration periods T_1 to T_6 considering a 5% viscous damping. These results are shown (values in blue) in Figs. 9–11 for the different water assumptions. The pseudo-acceleration spectra $S_A^{[\ddot{v}_g]}(T_j, 5\%)$, $j = 1 \dots 6$, corresponding to the original ground motions are also depicted (values in black) in the same figures. As expected, the hydrodynamic-induced modifications to acceleration seismic demands depend on the structural dynamic properties for each tower and the input ground motion. Table 2 contains the Hydrodynamic Modification Factor (HMF) obtained from Figs. 9–11 by dividing the values in blue by those in black for each vibration period.

From Figs. 9(a) and (c), it is seen that the acceleration demands corresponding to the fundamental modes of Cases nos. 1 and 2 without water are close when subjected to Imperial Valley ground motion (*i.e.* 0.61 and 0.57, respectively). These acceleration demands increase by 4% for Case no. 1 and 19% for Case no. 2 when hydrodynamic effects are included assuming compressible water. The larger amplification associated with Case no. 2 is mainly due to its higher flexibility compared to Case no. 1. Comparing Figs. 9(a) and (e), it is observed that the acceleration demand increase induced by hydrodynamic effects is 4% for both Cases nos. 1 and 3 when only the fundamental mode contribution is considered under the effect of Imperial Valley ground motion acceleration. Despite Case no. 3 being more flexible than Case

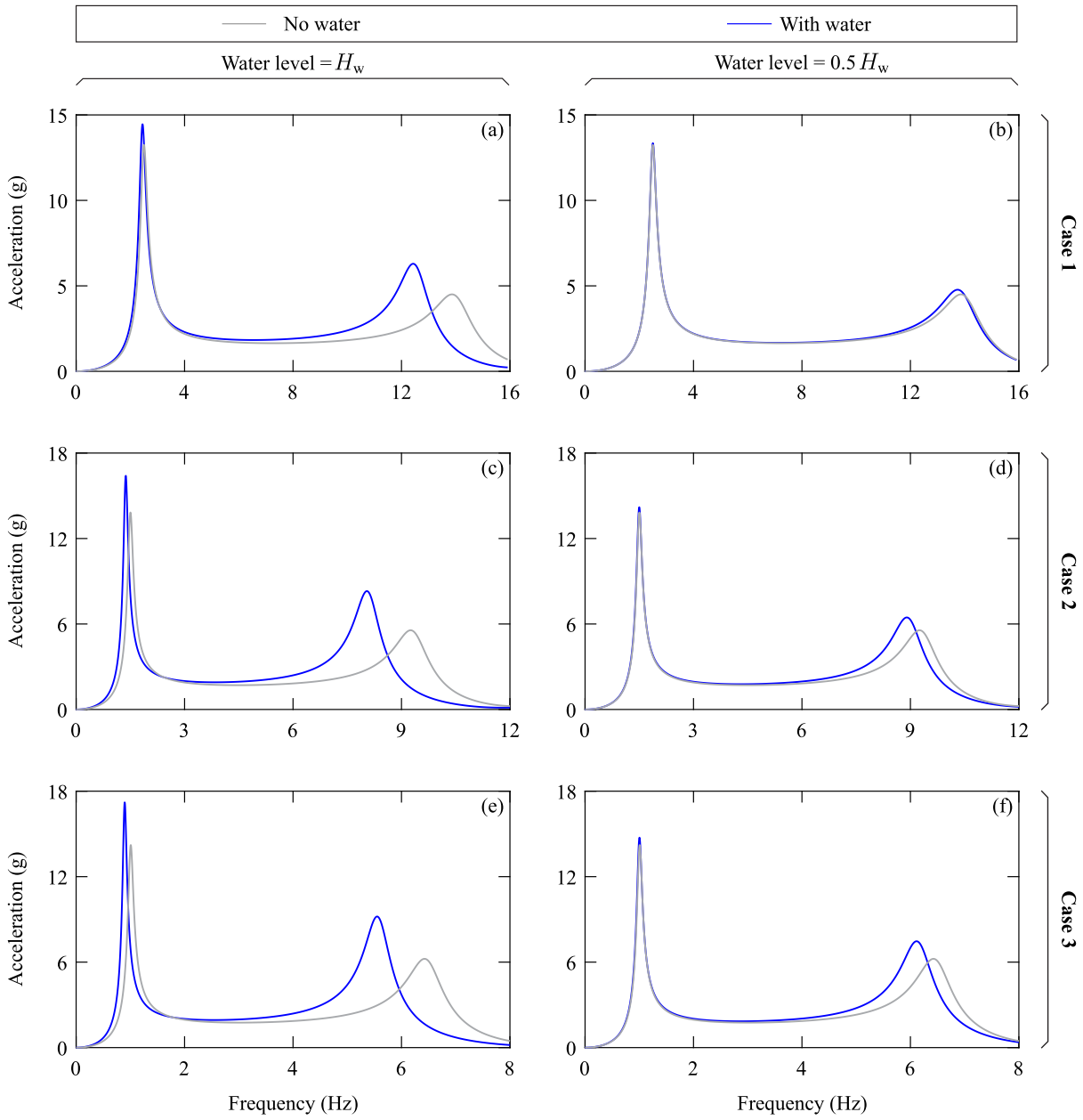


Fig. 5. Frequency response functions for horizontal acceleration $\ddot{\hat{u}}$ and $\ddot{u}$ at point A of the tower-water systems studied: (a) and (b): Tower Case no. 1 assuming water level to be H_w and $0.5H_w$, respectively; (c) and (d): Tower Case no. 2 assuming water level to be H_w and $0.5H_w$, respectively; (e) and (f): Tower Case no. 3 assuming water level to be H_w and $0.5H_w$, respectively;.

no. 1, the frequency shift caused by hydrodynamic effects has led to the same increase in acceleration demands for both structures.

Figs. 9(c) shows a 4% *decrease* in acceleration demand for Case no. 2 due to hydrodynamic effects in the third and fourth vibration modes when subjected to Imperial Valley ground motion acceleration. Conversely, the same structure undergoes a 33% *increase* in acceleration demand when subjected to Loma Prieta ground motion acceleration along the same modes (Figs. 9(d)). This effect is attributed to differences in the frequency content of input ground motion acceleration. The pseudo-acceleration response spectra assuming two added-masses formulation approaches are also given in Figs. 10 and 11 to illustrate the influence of water modelling assumptions. The assessment of the effects of water modelling assumptions can also be seen from Table 2 containing the HMFs obtained using Eq. (31) for six vibration modes of the towers and the ground motion accelerations considered. For example, it is seen that the increase in acceleration demands due to hydrodynamic effects are more pronounced when water is modelled using Morison added masses. Acceleration demands for Case no. 3 *decrease* along modes 5 and 6 due to hydrodynamic effects for Imperial Valley (1940) earthquake. In contrast, they *decrease* along the same modes when the tower is subjected to the Loma Prieta (1989) earthquake. The results in Table 2 can be used to assess the effectiveness of Morison's added masses across various vibration modes.

3.3. Seismic response of the water-surrounded axisymmetric structures

Fig. 12 presents the maximum absolute horizontal relative displacements obtained along the height of the towers subjected to the considered ground motions and assuming compressible water. The results corresponding to each mode are obtained using the proposed

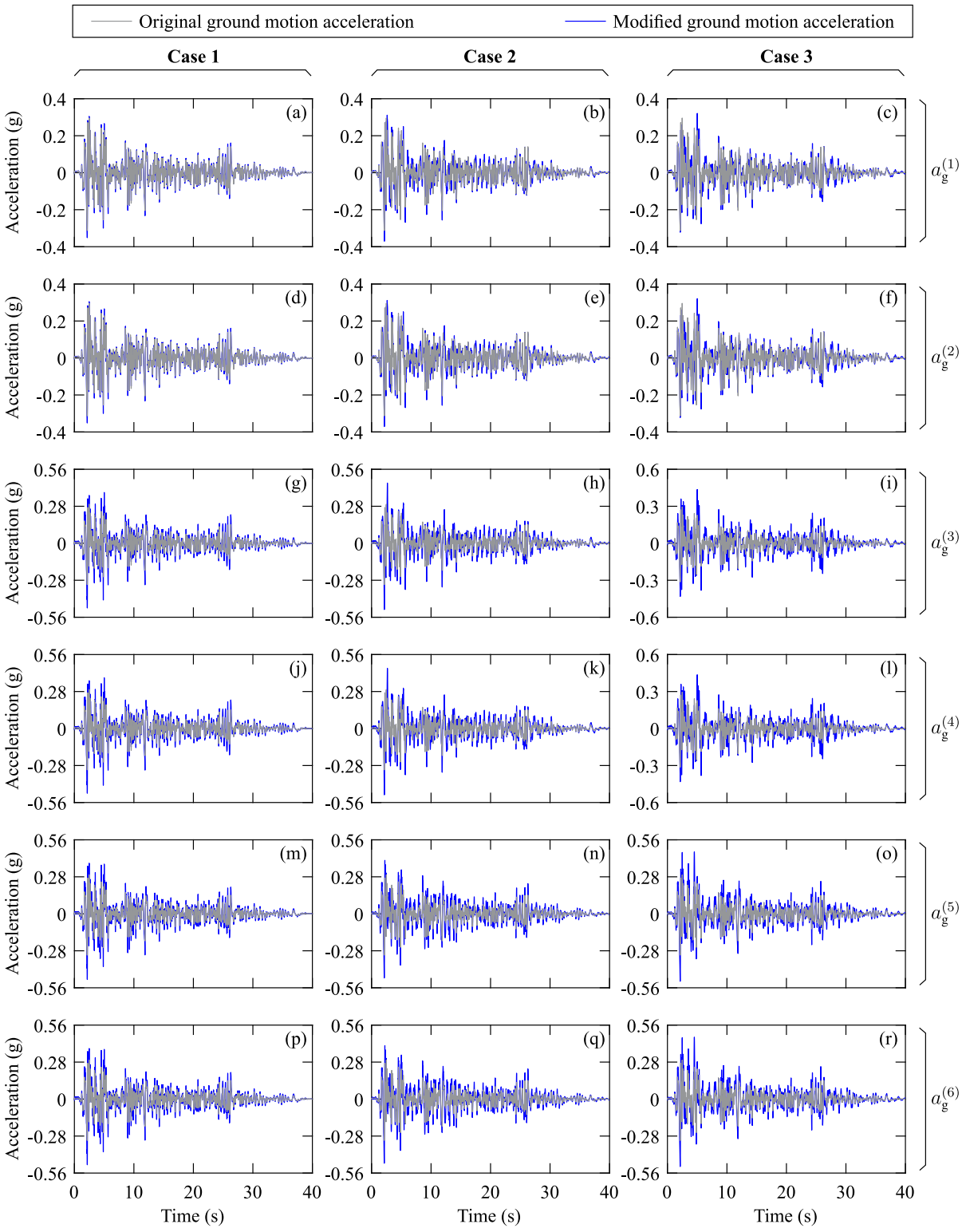


Fig. 6. Original and modified ground accelerations $a_g^{(1)}$ to $a_g^{(6)}$ corresponding to the six mode shapes of the 42 m (Case no. 1), 56 m (Case no. 2) and 70 m (Case no. 3) high towers, subjected to Imperial Valley (1940) earthquake with compressible water assumption.

response spectrum analysis (RSA). Figs. 13 and 14 show the results obtained using the proposed time–history analyses (THMSA). The results are in excellent agreement with those from the classical coupled finite element solutions. The total horizontal relative displacements at point A of the studied towers including hydrodynamic effects (compressible water assumption and added masses) are shown in Fig. 15 for the first twelve seconds of Imperial Valley (1940) and Loma Prieta (1989) earthquakes. A close match between the results for the compressible water assumption and the reference solution is found. The same observation applies to the results corresponding to the added mass formulation based on radiation waves theory. This observation is expected as the effects of water compressibility are known to be

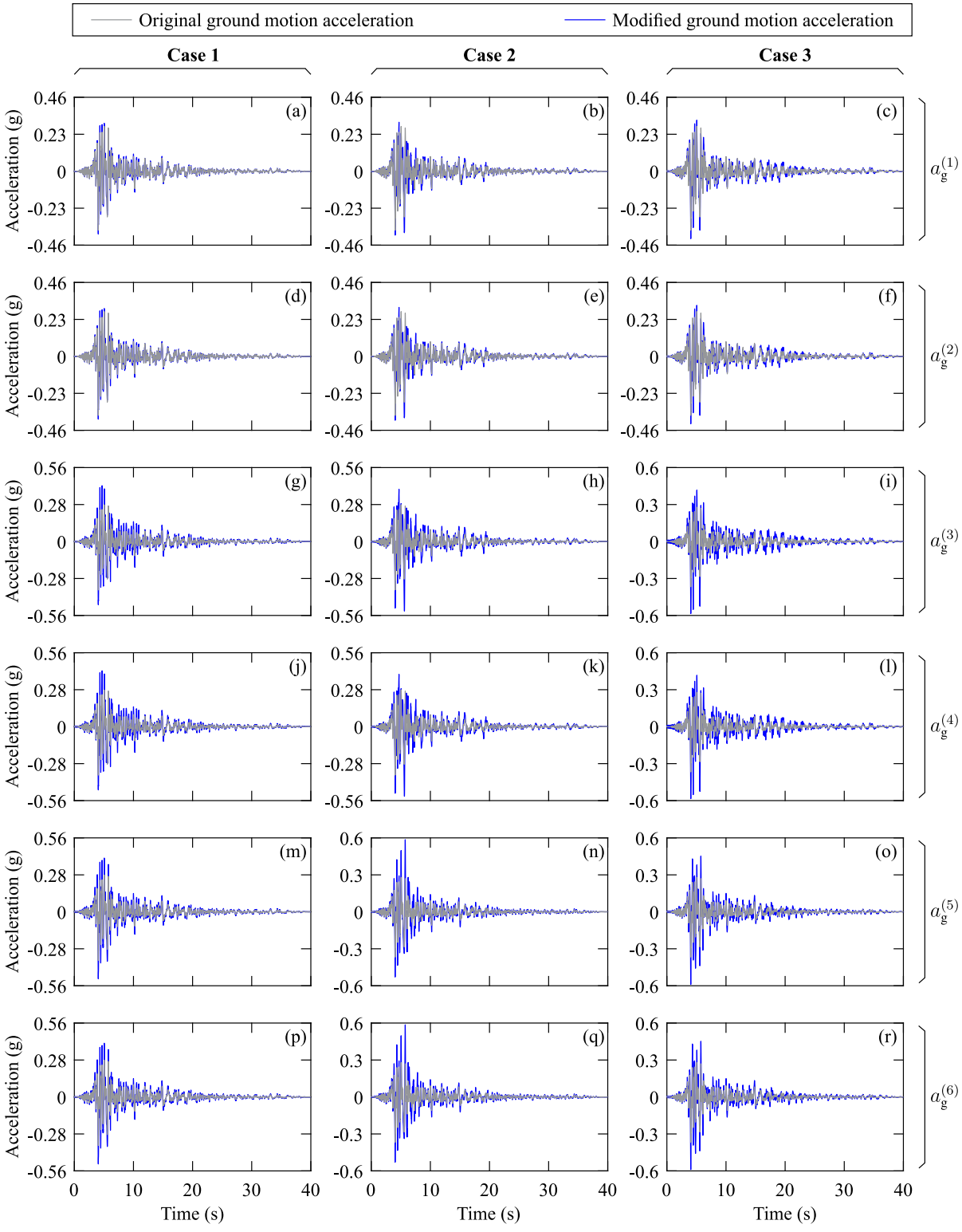


Fig. 7. Original and modified ground accelerations $a_g^{(1)}$ to $a_g^{(6)}$ corresponding to the six mode shapes of the 42 m (Case no. 1), 56 m (Case no. 2) and 70 m (Case no. 3) high towers, subjected to Loma Prieta (1989) earthquake with compressible water assumption.

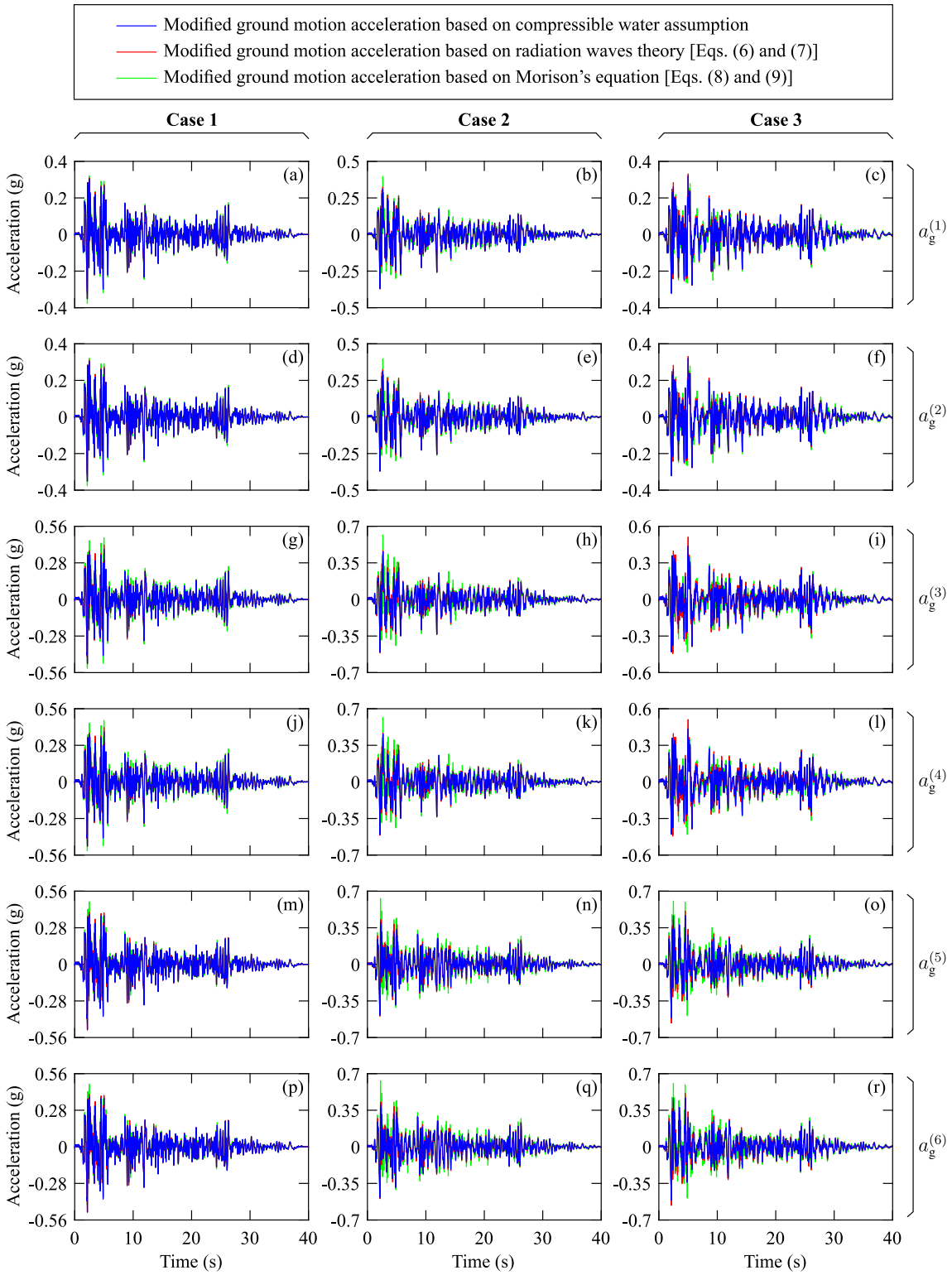


Fig. 8. Modified ground accelerations $a_g^{(1)}$ to $a_g^{(6)}$ corresponding to the selected six vibration modes of the studied towers subjected to Imperial Valley (1940) earthquake considering different water assumptions.

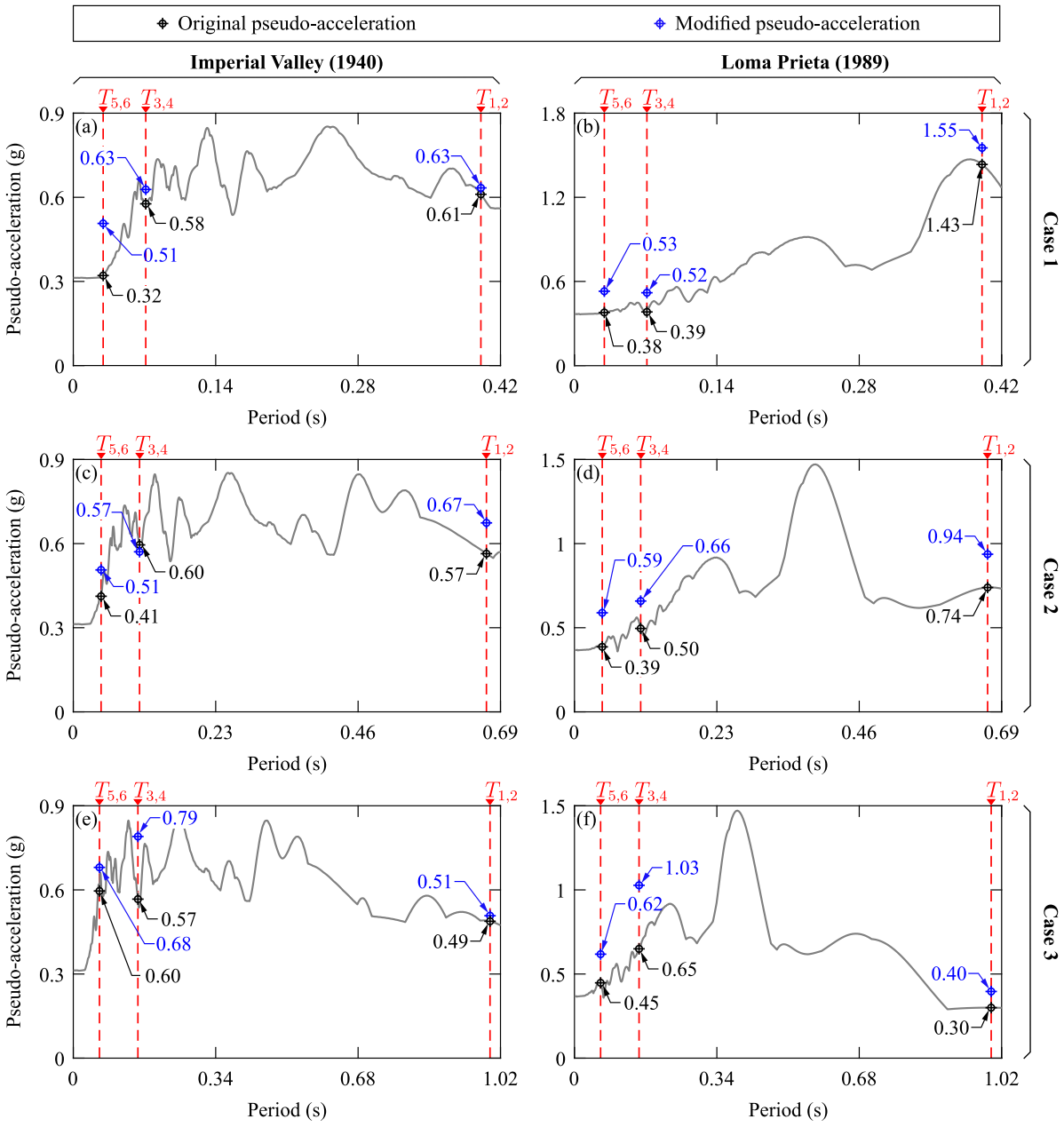


Fig. 9. 5%-damped pseudo-acceleration response spectra of the original ground motions and those of the modified ground motions corresponding to each of the selected six vibration modes assuming compressible water.

Table 2
Hydrodynamic modification factors obtained for the six vibration modes of tower Cases nos. 1, 2, and 3 subjected to the ground motion accelerations considered.

Case	Water assumption	Imperial Valley (1940)						Loma Prieta (1989)					
		Modes						Modes					
		1	2	3	4	5	6	1	2	3	4	5	6
No. 1	Compressible water	1.04	1.04	1.09	1.09	1.58	1.58	1.08	1.08	1.36	1.36	1.40	1.40
	Added masses — Eqs. (6)-(7)	1.03	1.03	1.15	1.15	1.60	1.60	1.08	1.08	1.27	1.27	1.40	1.40
	Added masses — Eqs. (8)-(9)	1.09	1.09	1.66	1.66	1.66	1.66	1.09	1.09	1.74	1.74	1.48	1.48
No. 2	Compressible water	1.19	1.19	0.96	0.96	1.23	1.23	1.27	1.27	1.33	1.33	1.52	1.52
	Added masses — Eqs. (6)-(7)	1.18	1.18	1.10	1.10	1.22	1.22	1.27	1.27	1.39	1.39	1.63	1.63
	Added masses — Eqs. (8)-(9)	1.26	1.26	2.17	2.17	1.96	1.96	1.29	1.29	1.61	1.61	1.92	1.92
No. 3	Compressible water	1.04	1.04	1.39	1.39	1.14	1.14	1.32	1.32	1.58	1.58	1.38	1.38
	Added masses — Eqs. (6)-(7)	1.03	1.03	1.55	1.55	0.98	0.98	1.32	1.32	1.48	1.48	1.57	1.57
	Added masses — Eqs. (8)-(9)	1.05	1.05	1.92	1.92	1.61	1.61	1.34	1.34	1.75	1.75	1.50	1.50

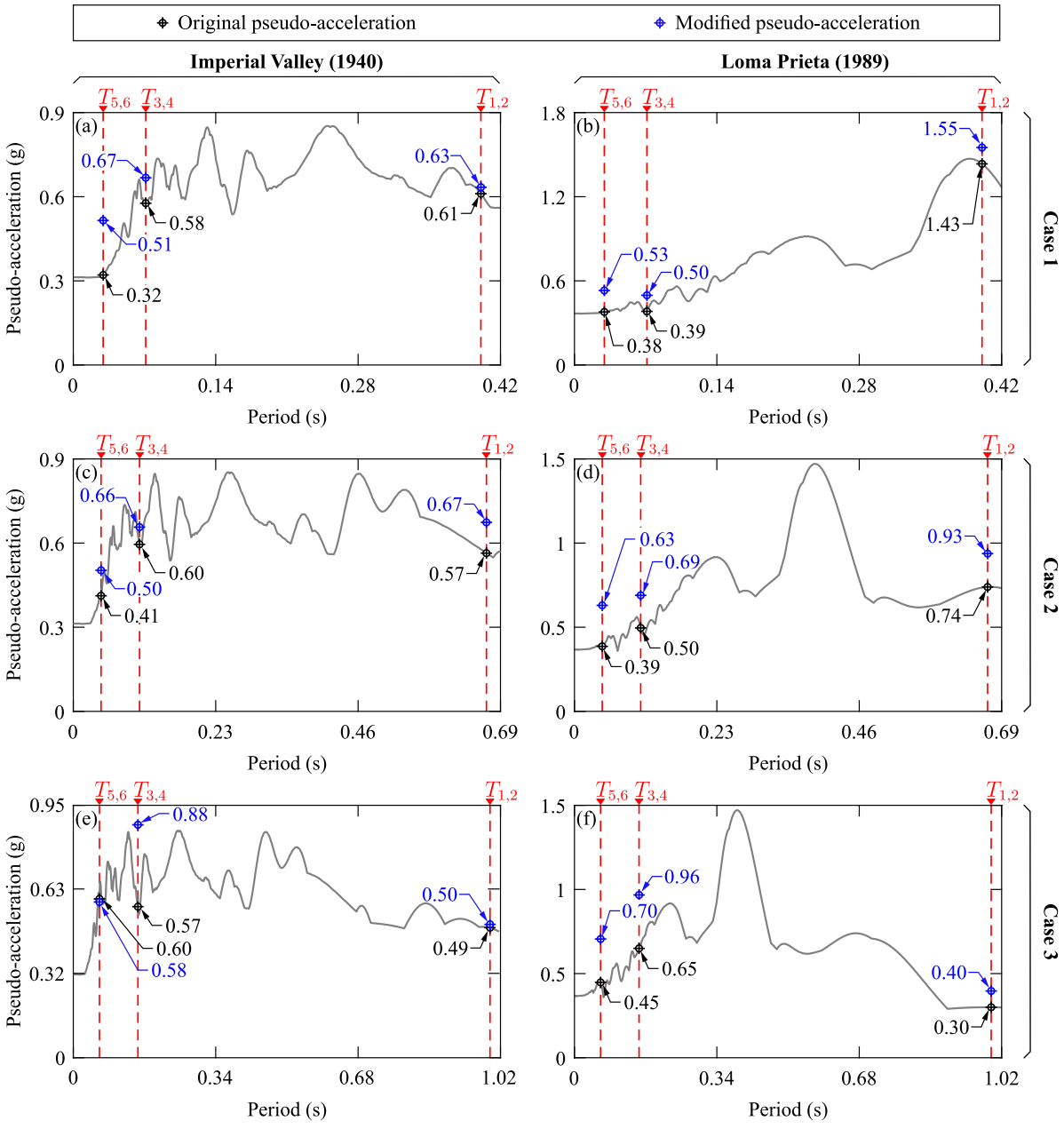


Fig. 10. 5%-damped pseudo-acceleration response spectra of the original ground motions and those of the modified ground motions corresponding to each of the six selected vibration modes obtained assuming simplified added mass formulation for the water surrounding the towers.

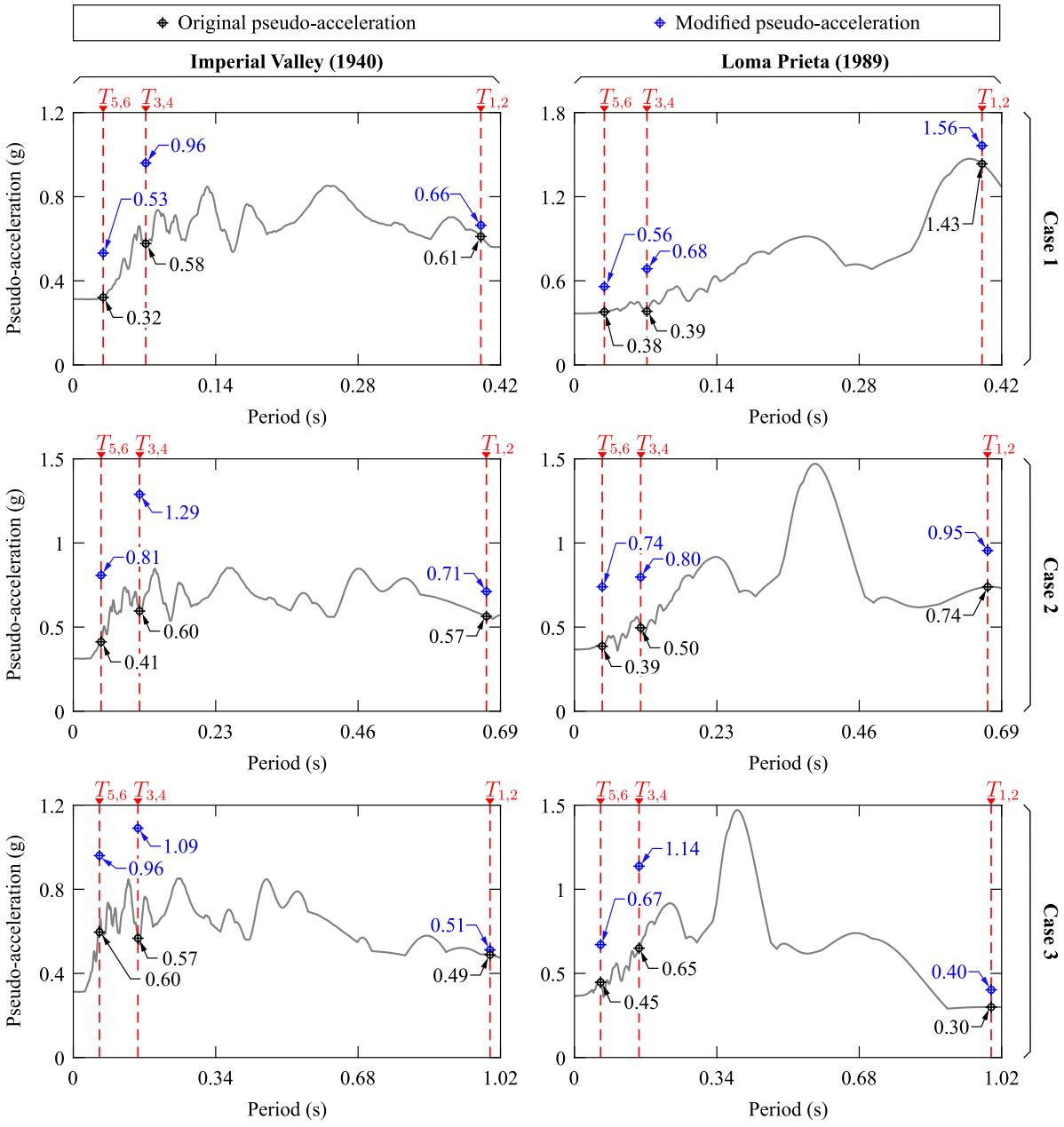


Fig. 11. 5%-damped pseudo-acceleration response spectra of the original ground motions and those of the modified ground motions corresponding to each of the six selected vibration modes obtained assuming Morison's added mass formulation for the water surrounding the towers.

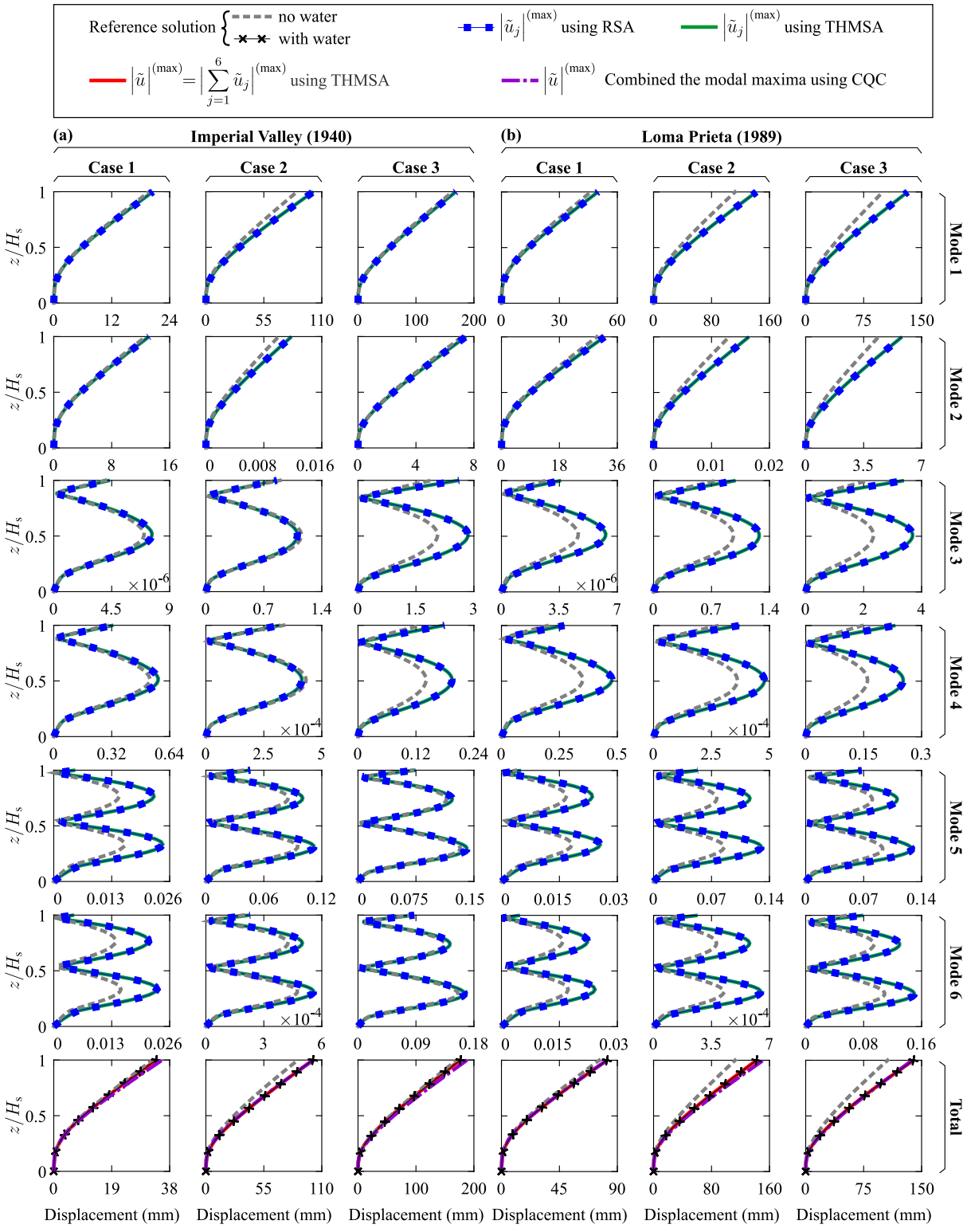


Fig. 12. Absolute maximum relative displacements along the height of the face of towers determined for each vibration mode using modified ground accelerations $a_g^{(1)}$ to $a_g^{(6)}$ and then combined to obtain total response: (a) Imperial Valley (1940) earthquake; (b) Loma Prieta (1989) earthquake obtained assuming compressible water.

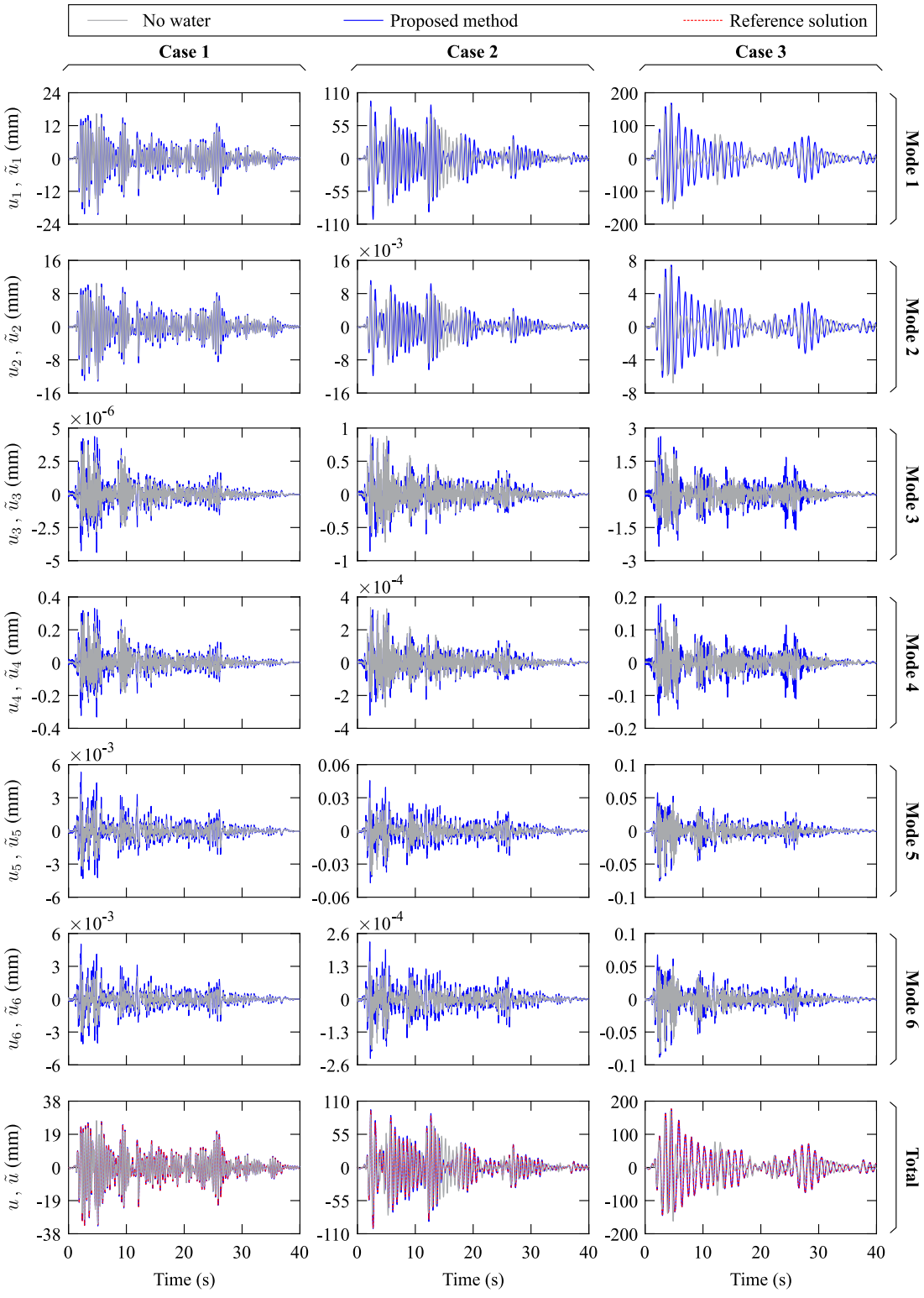


Fig. 13. Time-history horizontal relative displacements at point A of studied towers with hydrodynamic effects obtained for each vibration mode using modified ground accelerations $a_g^{(1)}$ to $a_g^{(6)}$ subjected to Imperial Valley (1940) earthquake assuming compressible water, and then combined to obtain total seismic response.

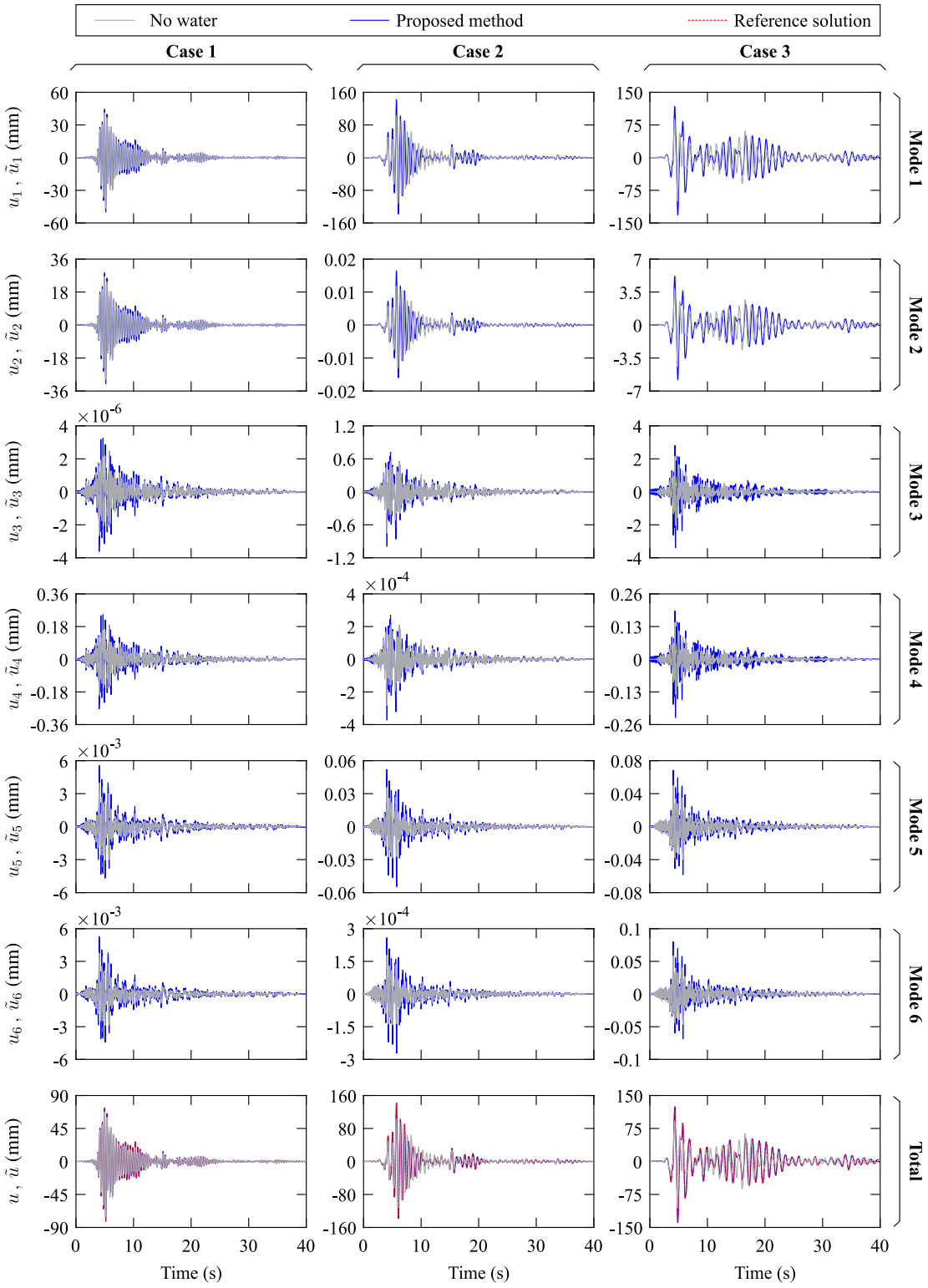


Fig. 14. Time-history horizontal relative displacements at point A of studied towers with hydrodynamic effects obtained for each vibration mode using modified ground accelerations $a_g^{(1)}$ to $a_g^{(6)}$ subjected to Loma Prieta (1989) earthquake assuming compressible water, and then combined to obtain total seismic response.

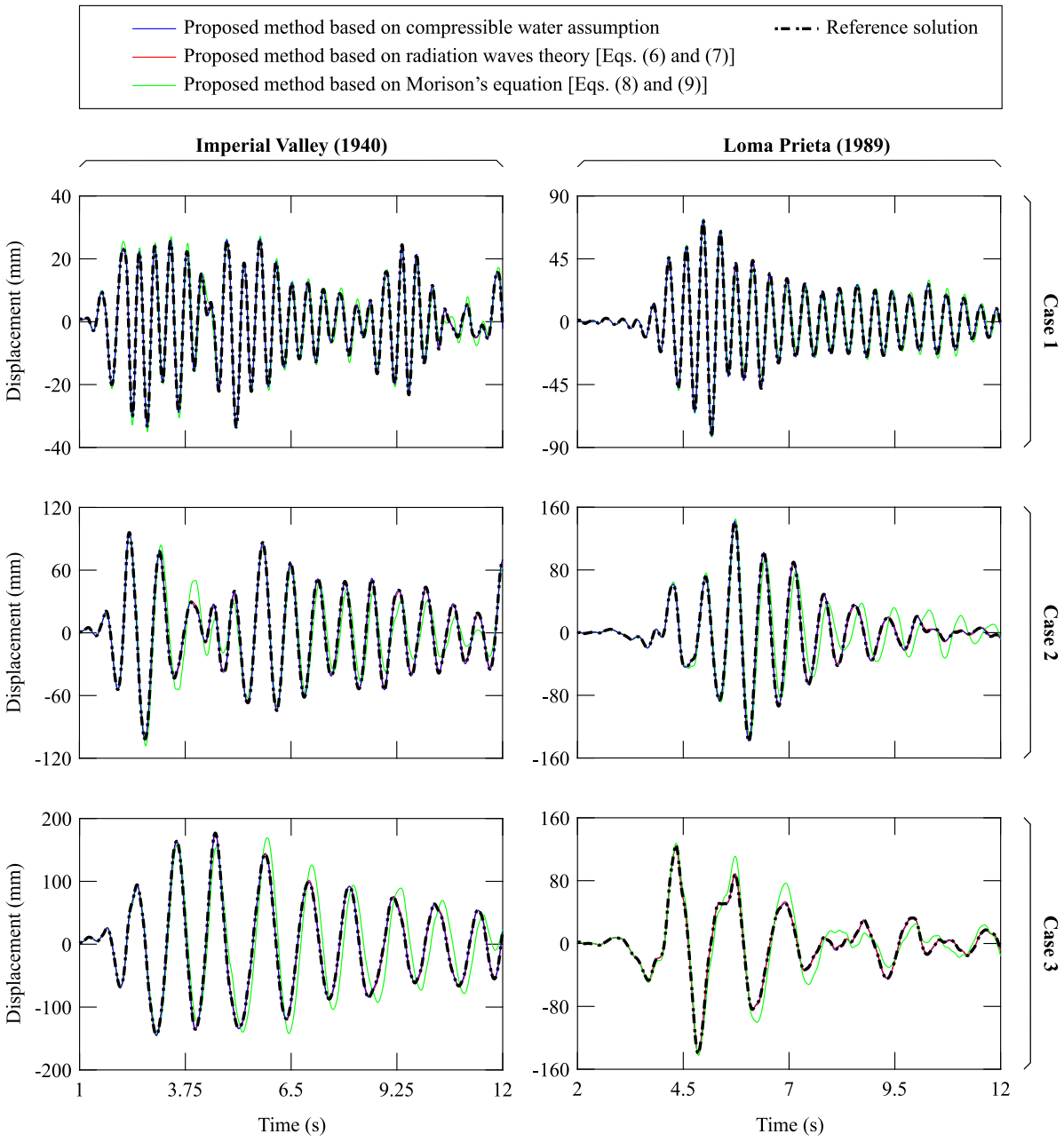


Fig. 15. Time-history of total horizontal relative displacements at point A of the studied towers including hydrodynamic effect considering Imperial Valley (1940) and Loma Prieta (1989) earthquakes obtained for different water assumptions.

negligible for this type of structures (*e.g.* Liaw and Chopra, 1974). Fig. 15 shows that the results corresponding to the added masses based on Morison's equation are slightly different from the others. The shear forces at the base of the towers (location S1 in Fig. 2) are also compared in Fig. 16 under the effect of Imperial Valley (1940) ground motion acceleration.

The maximum absolute total horizontal relative displacements shown in Figs. 12 (*i.e.* last row titled total) are obtained using two approaches: (i) a direct method consisting of the summation of the modal responses of horizontal relative displacements (*i.e.* algebraic values with signs) and then the computation of the maximum value of the resulting summed response, and (ii) the CQC method consisting of combining the absolute values of the maximum horizontal relative displacements obtained for each mode. As excepted, the results provided by the direct method are found to be identical to those of the reference solution. For both analysed earthquakes and the three studied towers, the CQC method exhibits slightly higher values than the direct method at the upper sections of the towers (*i.e.* $z/H_s > \approx 0.75$). However, at lower heights, the total maximum responses obtained through the CQC method are nearly identical to those from the direct method. Notably, for tower Case no. 1 subjected to Imperial Valley (1940) ground motion acceleration and towers Case no. 2 and Case no. 3 subjected to the Loma Prieta (1989) earthquake, the CQC method demonstrates excellent agreement with the reference solution.

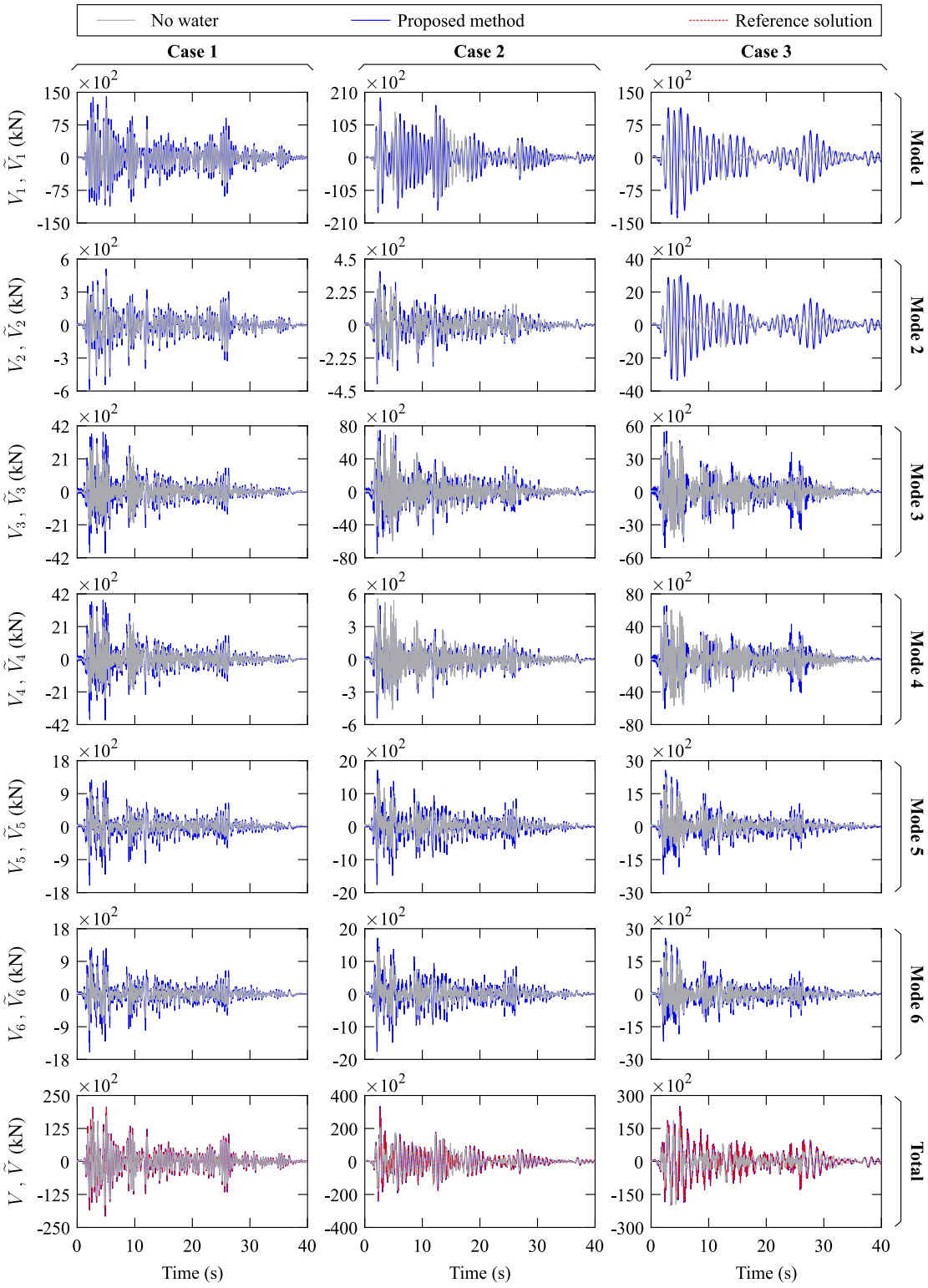


Fig. 16. Time-history shear force at the base of studied towers with surrounding water obtained for each vibration mode using modified ground accelerations $a_g^{(1)}$ to $a_g^{(6)}$ under the effect of Imperial Valley (1940) earthquake assuming compressible water, and then combined to obtain total seismic response.

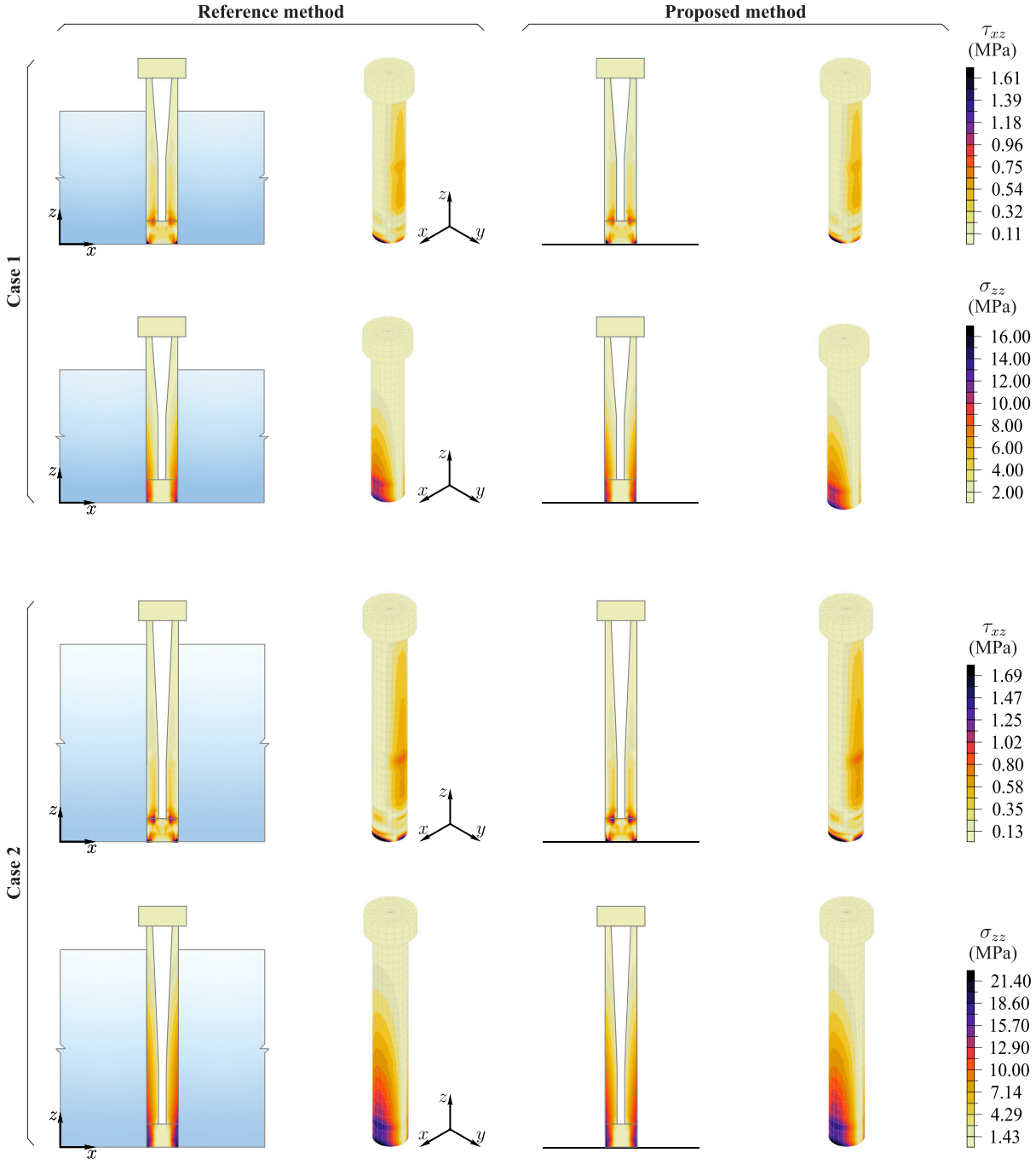


Fig. 17. Maximum shear stresses τ_{xz} and σ_{zz} developing within towers Case no. 1 and Case no. 2 subjected to Imperial Valley (1940) earthquake assuming compressible water.

Figs. 13 and 14 present the time–history horizontal relative displacements at point A of the towers under the effect of Imperial Valley (1940) and Loma Prieta (1989) ground motions, respectively. These results confirm the excellent agreement between the results obtained using the proposed methods and the classical coupled finite element solutions. Finally, the earthquake-induced stresses in the water-surrounded structure can be determined based on the time-histories of the nodal displacements computed using the proposed approach. For instance, the obtained maximum dynamic shear stress τ_{xz} and normal stress σ_{zz} within tower Cases no. 1 and no. 2 subjected to Imperial Valley (1940) earthquake and assuming compressible water are presented in Fig. 17. An excellent agreement with the stresses from the classical coupled finite element solutions is found.

4. Conclusions

This paper proposed novel methods to evaluate the seismic response of water-surrounded axisymmetric structures through dynamic modal superposition and response spectrum analyses. The developed techniques include earthquake-induced hydrodynamic effects into modified versions of the original ground motion acceleration and its response spectrum. The modified ground motion time–history and spectral accelerations can then be applied directly to the dry structure (*i.e.* without water), thus eliminating the need for specialized software accounting for fluid–structure interaction dynamic effects.

The proposed approach also allows the evaluation of the impact of any specific vibration mode and associated hydrodynamic effect on the structural seismic response. Coupled structural flexibility and hydrodynamic effects due to each vibration mode can be accurately assessed in lieu of the approximate results generally given by the static correction method commonly used in traditional simplified methods.

The methodology utilizes analytical formulations of earthquake-induced hydrodynamic pressure or simplified added-masses to obtain the contributions of the selected vibration modes to the total seismic response. It is shown that the developed methods also provide an alternative to the implementation of added masses by including their effects directly in the modified ground motion time–history or spectral accelerations.

Based on the formulations proposed, a hydrodynamic modification factor which can be used to evaluate the amplification or de-amplification of acceleration seismic demands due to earthquake-induced hydrodynamic effects was introduced. The proposed method can be applied to a broad range of axisymmetric structures surrounded by water, such as axisymmetric towers supporting wind turbines, intake towers, or bridge circular piers. For purpose of illustration, application examples of three water-surrounded axisymmetric structures subjected to two earthquakes were presented.

The obtained results were shown to be in excellent agreement with the coupled finite element solutions. The findings were discussed to highlight the coupled effects of hydrodynamic-pressure and structural flexibility on the seismic behaviour of the studied systems. Two main limitations of the proposed formulation are that the structures must be of cylindrical shape, and that the foundation is rigid. The rigid foundation assumption was adopted to focus on the modelling of the effects of water–structure interaction. The formulation presented can however be extended by including soil–structure interaction effects in the modal properties constituting the input of the proposed technique.

CRediT authorship contribution statement

Ramtin Kouhdasti: Writing – original draft, Visualization, Software, Methodology, Investigation, Formal analysis. **Najib Bouaanani:** Writing – review & editing, Writing – original draft, Visualization, Validation, Supervision, Software, Methodology, Investigation, Funding acquisition, Formal analysis, Conceptualization.

Declaration of competing interest

The authors declare that they have no known competing financial interests or personal relationships that could have appeared to influence the work reported in this paper.

Data availability

Data will be made available on request.

Acknowledgements

The authors would like to acknowledge the financial support of the Canada Research Chairs and the Natural Sciences and Engineering Research Council of Canada (NSERC).

Appendix

The FRFs p_0 and p_j, $j = 1 \cdots N_s$ can be evaluated as (Liaw and Chopra, 1974; Wei et al., 2015)

$$p_0(R_s,\theta,z,\omega) = \frac{4\rho_w}{H_w}\left[-\sum_{n=1}^{\bar{n}-1}\frac{I_{0n}}{\kappa_n}\mathcal{D}_n(\kappa_n R_s)\cos(\lambda_n z)\,e^{i\tau_n R_s} + \sum_{n=\bar{n}}^{N_w}\frac{I_{0n}}{\kappa'_n}\mathcal{E}_n(\kappa'_n R_s)\cos(\lambda_n z)\right]\cos(\theta) \tag{32}$$

$$p_j(R_s,\theta,z,\omega) = \frac{4\rho_w}{H_w}\left[-\sum_{n=1}^{\bar{n}-1}\frac{I_{jn}}{\kappa_n}\mathcal{D}_n(\kappa_n R_s)\cos(\lambda_n z)\,e^{i\tau_n R_s} + \sum_{n=\bar{n}}^{N_w}\frac{I_{jn}}{\kappa'_n}\mathcal{E}_n(\kappa'_n R_s)\cos(\lambda_n z)\right]\cos(\theta) \tag{33}$$

where N_w is the number of considered acoustical water modes, and the parameters λ_n, κ_n, κ'_n, I_{0n}, I_{jn}, $\mathcal{D}_n$, $\mathcal{E}_n$ and τ_n are given by

$$\lambda_n = \frac{(2n-1)\pi}{2H_w}; \qquad \kappa_n = \sqrt{\frac{\omega^2}{C_w^2}-\lambda_n^2}; \qquad \kappa'_n = -i\,\kappa_n \tag{34}$$

$$I_{0n} = -\frac{2H_w(-1)^n}{\pi(2n-1)}; \qquad I_{jn} = \int_0^{H_w}\psi_j^{(x)}(z)\,\cos(\lambda_n z)\,dz \tag{35}$$

$$\mathcal{D}_n(\kappa_n R_s) = \sqrt{\frac{\left[J_1(\kappa_n R_s)\right]^2+\left[Y_1(\kappa_n R_s)\right]^2}{\left[J_0(\kappa_n R_s)-J_2(\kappa_n R_s)\right]^2+\left[Y_0(\kappa_n R_s)-Y_2(\kappa_n R_s)\right]^2}} \tag{36}$$

$$\mathcal{E}_n(\kappa'_n R_s) = \frac{K_1(\kappa'_n R_s)}{K_0(\kappa'_n R_s)+K_2(\kappa'_n R_s)} \tag{37}$$

$$\tau_n R_s = \tan^{-1}\left\{\frac{\left[Y_0(\kappa_n R_s)-Y_2(\kappa_n R_s)\right]J_1(\kappa_n R_s)-\left[J_0(\kappa_n R_s)-J_2(\kappa_n R_s)\right]Y_1(\kappa_n R_s)}{\left[J_0(\kappa_n R_s)-J_2(\kappa_n R_s)\right]J_1(\kappa_n R_s)+\left[Y_0(\kappa_n R_s)-Y_2(\kappa_n R_s)\right]Y_1(\kappa_n R_s)}\right\} \tag{38}$$

in which K_ℓ is the modified Bessel function of order ℓ of the second kind and J_ℓ and Y_ℓ are the Bessel functions of order ℓ of the first and second kind, respectively. The integer $\bar{n}$ in the first sums of Eqs. (32) and (33) is the smallest value of integer n such that $\lambda_n > \frac{\omega}{C_w}$. We note that the first series in Eqs. (32) and (33) vanishes if $\bar{n} = 1$. If water compressibility is neglected, the frequency-independent hydrodynamic pressure solutions p_0 and p_j given by Eq. (32) and (33) can be simplified to

$$p_0(R_s,z,\theta) = \sum_{n=1}^{N_w}\frac{4\rho_w}{H_w}\frac{I_{0n}}{\kappa'_n}\mathcal{E}_n(\kappa'_n R_s)\cos(\lambda_n z)\cos(\theta) \tag{39}$$

$$p_j(R_s,z,\theta) = \sum_{n=1}^{N_w}\frac{4\rho_w}{H_w}\frac{I_{jn}}{\kappa'_n}\mathcal{E}_n(\kappa'_n R_s)\cos(\lambda_n z)\cos(\theta) \tag{40}$$

in which λ_n, I_{0n}, I_{jn} and $\mathcal{E}_n(\kappa'_n R_s)$ are given by Eqs. (34), (35) and (37), respectively, and

$$\kappa'_n = \frac{(2n-1)\pi}{2H_w} \tag{41}$$

References

ADINA, R., 2022. Theory and modeling guide, rep. no. ARD 06–7.. Watertown MA.

Alembagheri, M., 2017. Frequency domain analysis of submerged tower-dam dynamic interaction. Soil Mech. Found. Eng. 54, 264–275.

Bigdeli, A., Akbari, H., Alembagheri, M., Haghgou, H., Matinfar, M., 2023. Influence of near-field ground motions and their equivalent pulses on nonlinear seismic response of intake-outlet towers and predicting based on artificial neural networks. In: Structures, Vol. 52. Elsevier, pp. 1051–1070.

Bouaanani, N., Lu, F.Y., 2009. Assessment of potential-based fluid finite elements for seismic analysis of dam–reservoir systems. Comput. Struct. 87 (3–4), 206–224.

Bouaanani, N., Perrault, C., 2010. Practical formulas for frequency domain analysis of earthquake-induced dam-reservoir interaction. J. Eng. Mech. 136 (1), 107–119.

Chen, B.-F., 2000. Dynamic responses of coastal structures during earthquakes including sediment–sea–structure interaction. Soil Dyn. Earthq. Eng. 20 (5–8), 445–467.

Czygan, O., Von Estorff, O., 2002. Fluid-structure interaction by coupling BEM and nonlinear FEM. Eng. Anal. Bound. Elem. 26 (9), 773–779.

Everstine, G., 1981. A symmetric potential formulation for fluid-structure interaction. J. Sound Vib. 79 (1), 157–160.

Fenves, G., Chopra, A.K., 1984. Earthquake analysis of concrete gravity dams including reservoir bottom absorption and dam-water-foundation rock interaction. Earthq. Eng. Struct. Dyn. 12 (5), 663–680.

Goyal, A., Chopra, A.K., 1989. Earthquake analysis of intake-outlet towers including tower-water-foundation-soil interaction. Earthq. Eng. Struct. Dyn. 18 (3), 325–344.

Greenhow, M., Yanbao, L., 1987. Added masses for circular cylinders near or penetrating fluid boundaries-review, extension and application to water-entry, -exit and slamming. Ocean Eng. 14 (4), 325–348.

Guo, J., Zhao, M., Wang, P., Zhang, N., 2021. Comparative assessment of simplified methods for hydrodynamic force on cylinder under earthquakes. Ocean Eng. 234, 109219.

Han, H., Guo, Y., Huo, R., 2023. Semi-analytical solution of transverse vibration of cylinders with non-circular cross-section partially submerged in water. J. Marine Sci. Eng. 11 (4), 872.

Huang, Y., Zhao, M., Wang, P., Cheng, X., Du, X., 2023. Analytical solution of dynamic responses of offshore wind turbine supported by monopile under combined earthquake, wave and wind. Ocean Eng. 267, 113319.

Jiang, H., Wang, B., Bai, X., Zeng, C., Zhang, H., 2017. Simplified expression of hydrodynamic pressure on deepwater cylindrical bridge piers during earthquakes. J. Bridge Eng. 22 (6), 04017014.

Li, Y., Li, Z., Wu, Q., 2017. Experiment and calculation method of the dynamic response of deep water bridge in earthquake. Latin Am. J. Solids Struct. 14 (13), 2518–2533.

Li, Q., Yang, W., 2013. An improved method of hydrodynamic pressure calculation for circular hollow piers in deep water under earthquake. Ocean Eng. 72, 241–256.

Li, Z.-X., Zheng, Q., Wu, K., Shi, Y., 2022. Seismic analysis and test facilities of deep-water bridges considering water-structure interaction: A state-of-the-art review. Earthq. Eng. Resilience 1 (1), 21–39.

Liaw, C.-Y., Chopra, A.K., 1974. Dynamics of towers surrounded by water. Earthq. Eng. Struct. Dyn. 3 (1), 33–49.

Liu, J., Lin, G., 2013. Numerical modelling of wave interaction with a concentric cylindrical system with an arc-shaped porous outer cylinder. Eur. J. Mech. B Fluids 37, 59–71.

Liu, C.-g., Sun, G.-s., 2014. Calculation and experiment for dynamic response of bridge in deep water under seismic excitation. China Ocean Eng. 28 (4), 445–456.

Lu, J.-F., Jeng, D.-S., 2010. Dynamic response of an offshore pile to pseudo-stoneley waves along the interface between a poroelastic seabed and seawater. Soil Dyn. Earthq. Eng. 30 (4), 184–201.

Meng, X.-N., Zou, Z.-J., 2012. Wave interaction with a uniform porous cylinder of arbitrary shape. Ocean Eng. 44, 90–99.

Millán, M., Young, Y., Prevost, J., 2009. Seismic response of intake towers including dam–tower interaction. Earthq. Eng. Struct. Dyn. 38 (3), 307–329.

Morison, J., Johnson, J.W., Schaaf, S.A., 1950. The force exerted by surface waves on piles. J. Pet. Technol. 2 (05), 149–154.

Olson, L.G., Bathe, K.-J., 1985. Analysis of fluid-structure interactions. a direct symmetric coupled formulation based on the fluid velocity potential. Comput. Struct. 21 (1–2), 21–32.

Padrón, L.A., Carbonari, S., Dezi, F., Morici, M., Bordón, J.D., Leoni, G., 2022. Seismic response of large offshore wind turbines on monopile foundations including dynamic soil–structure interaction. Ocean Eng. 257, 111653.

Penzien, J., Kaul, M., 1972. Response of offshore towers to strong motion earthquakes. Earthq. Eng. Struct. Dyn. 1 (1), 55–68.

Sigrist, J.-F., Garreau, S., 2007. Dynamic analysis of fluid–structure interaction problems with modal methods using pressure-based fluid finite elements. Finite Elem. Anal. Des. 43 (4), 287–300.

Sun, B., Zhang, S., Cui, W., Deng, M., Wang, C., 2020. Nonlinear dynamic response and damage analysis of hydraulic arched tunnels subjected to p waves with arbitrary incoming angles. Comput. Geotech. 118, 103358.

Tanaka, Y., Hudspeth, R.T., 1988. Restoring forces on vertical circular cylinders forced by earthquakes. Earthq. Eng. Struct. Dyn. 16 (1), 99–119.

Tao, L., Song, H., Chakrabarti, S., 2007. Scaled boundary FEM solution of short-crested wave diffraction by a vertical cylinder. Comput. Methods Appl. Mech. Engrg. 197 (1–4), 232–242.

Taylor, R.E., Duncan, P., 1980. Fluid-induced inertia and damping in vibrating offshore structures. Appl. Ocean Res. 2 (1), 3–12.

Tian, Z., Liu, F., Zhou, L., Yuan, C., 2020. Fluid-structure interaction analysis of offshore structures based on separation of transferred responses. Ocean Eng. 195, 106598.

Wang, P., Long, P., Zhao, M., Zhang, C., Du, X., 2021. Analytical solution of earthquake-induced hydrodynamic pressure on arrays of circular cylinders considering high-order scattered waves. J. Eng. Mech. 147 (9), 04021051.

Wang, P., Zhang, C., Wang, X., Zhao, M., Du, X., 2022. An accurate and efficient time-domain numerical model for simulating water-axisymmetric structure subjected to horizontal earthquakes. Mar. Struct. 85, 103234.

Wang, P., Zhao, M., Du, X., Liu, J., Chen, J., 2018a. Simplified evaluation of earthquake-induced hydrodynamic pressure on circular tapered cylinders surrounded by water. Ocean Eng. 164, 105–113.

Wang, P., Zhao, M., Li, H., Du, X., 2018b. An accurate and efficient time-domain model for simulating water-cylinder dynamic interaction during earthquakes. Eng. Struct. 166, 263–273.

Wei, K., Bouaanani, N., Yuan, W., 2015. Simplified methods for efficient seismic design and analysis of water-surrounded composite axisymmetric structures. Ocean Eng. 104, 617–638.

Westergaard, H.M., 1933. Water pressures on dams during earthquakes. Trans. Am. Soc. Civil Eng. 98 (2), 418–433.

Williams, A.N., 1986. Earthquake response of submerged circular cylinder. Ocean Eng. 13 (6), 569–585.

Wu, K., Li, N., Li, Z., 2023a. An extended multiple-support response spectrum method incorporating fluid-structure interaction for seismic analysis of deep-water bridges. Earthq. Eng. Eng. Vibr. 22 (1), 211–223.

Wu, K., Ma, J., Chen, Y., Huang, X., Qi, L., Li, C., 2023b. Study on the hydrodynamic added mass of rectangular pier under sine wave actions. In: Structures, Vol. 54. Elsevier, pp. 1371–1380.

Xu, L.-Y., Song, C.-X., Cai, F., Chen, W.-Y., Xue, Y.-Y., Chen, G.-X., 2023. An integrated model for offshore wind turbine monopile in porous seabed under multi-directional seismic excitations. Ocean Eng. 285, 115250.

Yang, W., Li, Q., 2013. The expanded morison equation considering inner and outer water hydrodynamic pressure of hollow piers. Ocean Eng. 69, 79–87.

Yang, W., Li, Q., Yeh, H., 2017. Calculation method of hydrodynamic forces on circular piers during earthquakes. J. Bridge Eng. 22 (11), 04017093.

Zhang, J., Wei, K., Qin, S., 2019. An efficient numerical model for hydrodynamic added mass of immersed column with arbitrary cross-section. Ocean Eng. 187, 106192.

Zheng, X.Y., Li, H., Rong, W., Li, W., 2015. Joint earthquake and wave action on the monopile wind turbine foundation: An experimental study. Mar. Struct. 44, 125–141.